Desalination 287 (2012) 2–18

Contents lists available at SciVerse ScienceDirect

Desalination

journal homepage: www.elsevier.com/locate/desal

Membrane distillation: A comprehensive review

Abdullah Alkhudhiri [a], Naif Darwish [b], Nidal Hilal [a,c,*]

[a] Centre Water Advanced Technologies and Environmental Research (CWATER), College of Engineering, Swansea University, Swansea SA2 8PP, UK
[b] American University of Sharjah, College of Engineering, Department of Chemical Engineering, Sharjah, P.O. Box 26666, United Arab Emirates
[c] Masdar Institute of Science and Technology, Abu Dhabi, United Arab Emirates

ARTICLE INFO

Article history:
Received 16 June 2011
Received in revised form 10 August 2011
Accepted 11 August 2011
Available online 16 September 2011

Keywords:
Desalination
Membrane distillation
AGMD
Membrane

ABSTRACT

Membrane Distillation (MD) is a thermally-driven separation process, in which only vapour molecules transfer through a microporous hydrophobic membrane. The driving force in the MD process is the vapour pressure difference induced by the temperature difference across the hydrophobic membrane. This process has various applications, such as desalination, wastewater treatment and in the food industry.
This review addresses membrane characteristics, membrane-related heat and mass transfer concepts, fouling and the effects of operating condition. State of the art research results in these different areas will be presented and discussed.

Contents

* Corresponding author. Tel.: +44 1792 606644.
E-mail address: n.hilal@swansea.ac.uk (N. Hilal).

0011-9164/$ – see front matter
doi:10.1016/j.desal.2011.08.027

1. Introduction

Supply and demand for fresh water have increased gradually in the last two decades. In this context, Membrane Distillation (MD) is a promising technology for desalting highly saline waters. MD is a thermally-driven separation (microfiltration) process, in which only vapour molecules are able to pass through a porous hydrophobic membrane. This separation process is driven by the vapour pressure difference existing between the porous hydrophobic membrane surfaces. Using MD has many attractive features, such as low operating temperatures in comparison to those encountered in conventional process; the solution (mainly water) is not necessarily heated up to the boiling point. Moreover, the hydrostatic pressure encountered in MD is lower than that used in pressure-driven membrane processes like reverse osmosis (RO). Therefore, MD is expected to be a cost-effective process, which requires less demanding of membrane characteristics too. In this respect, less expensive material can be involved in it such as plastic, for example, thus alleviating corrosion problems. According to the principle of vapour–liquid equilibrium, the MD process has a high rejection factor. As a matter of fact, theoretically, complete separation takes place. In addition, the membrane pore size required for MD is relatively larger than those for other membrane separation processes, such as RO. The MD process, therefore, suffers less from fouling. The MD system has the feasibility to be combined with other separation processes to create an integrated separation system, such as ultrafiltration (UF) [1] or with a RO unit [2]. Furthermore, MD has the ability to utilise alternative energy sources, such as solar energy [3,4]. The MD process is competitive for desalination of brackish water and sea water [5]. It is also an effective process for removing organic and heavy metals from aqueous solution [6], from waste water [7]. MD has also been used to treat radioactive waste, where the product could be safely discharged to the environment [8]. However, MD is also attended by some drawbacks such as low permeate flux (compared to other separation processes, like RO), high susceptibility permeate flux to the concentration and temperature of the feed conditions due to the concentration and temperature polarization phenomenon. Also, the trapped air within the membrane introduces a further mass transfer resistance, which also limits the MD permeate flux. Moreover, the heat lost by conduction is quite large.

Mass transfer in MD is controlled by three basic mechanisms, which are Knudsen diffusion, Poiseuille flow (viscous flow) and molecular diffusion. This gives rise to several types of resistance to mass transfer resulting from transfer of momentum to the supported membrane (viscous), collision of molecules with other molecules (molecular resistance) or with the membrane itself-(Knudsen resistance (see Fig. 1). In this context, the dusty gas model is used to describe the mass transfer resistances in the MD system. It is worth mentioning that the mass transfer boundary layer resistance is generally negligible [9]. Similarly, the surface resistance is insignificant, because the surface area of the MD is small compared to the pore area. On the other hand, the thermal boundary layer is considered to be the factor limiting mass transfer [9,10].

2. Membrane configuration

In this section, different MD configurations that have been utilized to separate aqueous feed solution using a microporous hydrophobic membrane will be addressed.

2.1. Direct Contact Membrane Distillation (DCMD)

In this configuration (Fig. 2), the hot solution (feed) is in direct contact with the hot membrane side surface. Therefore, evaporation takes place at the feed-membrane surface. The vapour is moved by the pressure difference across the membrane to the permeate side and condenses inside the membrane module. Because of the hydrophobic characteristic, the feed cannot penetrate the membrane (only the gas phase exists inside the membrane pores). DCMD is the simplest MD configuration, and is widely employed in desalination processes and concentration of aqueous solutions in food industries, [11–15] or acids manufacturing [16]. The main drawback of this design is the heat lost by conduction.

2.2. Air Gap Membrane Distillation (AGMD)

The schematic of the Air Gap Membrane Distillation (AGMD) is shown in Fig. 3. The feed solution is in direct contact with the hot side of the membrane surface only. Stagnant air is introduced between the membrane and the condensation surface. The vapour crosses the air gap to condense over the cold surface inside the membrane cell. The benefit of this design is the reduced heat lost by conduction. However, additional resistance to mass transfer is created, which is considered a disadvantage. This configuration is suitable for desalination [5,17] and removing volatile compounds from aqueous solutions [6,18,19].

2.3. Sweeping Gas Membrane Distillation (SGMD)

In Sweeping Gas Membrane Distillation (SGMD), as the schematic diagram in Fig. 4 shows, inert gas is used to sweep the vapour at the permeate membrane side to condense outside the membrane module. There is a gas barrier, like in AGMD, to reduce the heat loss, but this is not stationary, which enhances the mass transfer coefficient. This configuration is useful for removing volatile compounds from

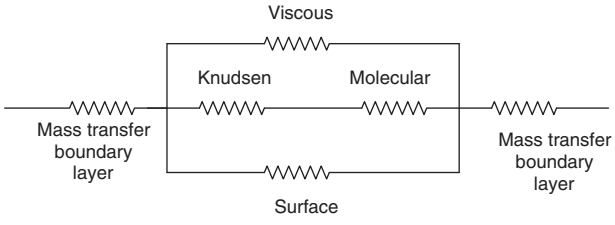

Fig. 1. Mass transfer resistances in MD.

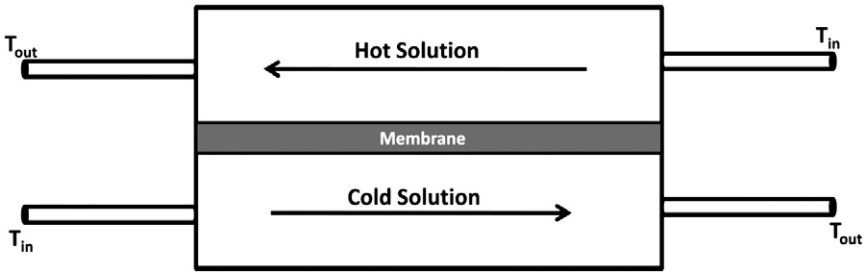

Fig. 2. Direct Contact Membrane Distillation (DCMD).

aqueous solution [17]. The main disadvantage of this configuration is that a small volume of permeate diffuses in a large sweep gas volume, requiring a large condenser.

It is worthwhile stating that AGMD and SGMD can be combined in a process called thermostatic sweeping gas membrane distillation (TSGMD). The inert gas in this case is passed through the gap between the membrane and the condensation surface. Part of vapour is condensed over the condensation surface (AGMD) and the remainder is condensed outside the membrane cell by external condenser (SGMD). [20,21].

2.4. Vacuum Membrane Distillation (VMD)

The schematic diagram of this module is shown in Fig. 5. In VMD configuration, a pump is used to create a vacuum in the permeate membrane side. Condensation takes place outside the membrane module. The heat lost by conduction is negligible, which is considered a great advantage [10]. This type of MD is used to separate aqueous volatile solutions [22–24].

3. Membrane characteristics

Hydrophobic (non-wetting) microporous membranes are used in the MD process. These membranes are made from polytetrafluoroethylene (PTFE), polypropylene (PP) or polyvinylidene fluoride (PVDF). In general, the membrane used in the MD system should have low resistance to mass transfer and low thermal conductivity to prevent heat loss across the membrane. In addition, the membrane should have good thermal stability in extreme temperatures, and high resistance to chemicals, such as acids and bases.

3.1. Liquid entry pressure (wetting pressure)

Liquid entry pressure (LEP) is a significant membrane characteristic. The feed liquid must not penetrate the membrane pores; so the pressure applied should not exceed the limit, or LEP, where the liquid (i.e. aqueous solution) penetrates the hydrophobic membrane. LEP depends on the maximum pore size and the membrane hydrophobicity. It is directly related to feed concentration and the presence of organic solutes, which usually reduce the LEP. For example, LEP linearly decreases when ethanol concentration increases in the solution [25]. In addition, Garcia-Payo et al. [26] indicated that LEP is strongly dependent on the alcohol type, alcohol concentration in the aqueous solution, and solution temperature.

According to Franken et al. [27], LEP can be estimated from Eq. (1):

$$\Delta P = P_f - P_p = \frac{-2B\gamma_l \cos\theta}{r_{max}} \quad (1)$$

where P_f *and* P_p are the hydraulic pressure on the feed and permeate side, B is a geometric pore coefficient (equal to 1 for cylindrical pores), γ_l is liquid surface tension, θ contact angle and r_{max} is the maximum pore size. The contact angle of a water droplet on a Teflon surface varies from 108° to 115°; 107° for PVDF [9,28] and 120° for PP [9]. It is worthwhile indicating that a flat ceramic membrane made by S. Khemakhem and R. Ben Amar [29] had a contact angle varying from 177° to 179°. Moreover, ceramic zirconia and titania hydrophobic membranes were prepared with a 160° contact angle [30]. All these ceramic membranes are used for desalination purposes (see Table 1).

With regard to surface tension, Zianhua et al. [31] studied the impact of salt concentration (NaCl) on the water surface tension and found that:

$$\gamma_{l\_new} = \gamma_l + 1.467\, c_f \quad (2)$$

γ_l stands for pure water surface tension at 25 °C, which is 72 mN/m.

As a result, membranes that have a high contact angle (high hydrophobicity), small pore size, low surface energy and high surface tension for the feed solution possess a high LEP value [32]. Typical values for surface energy for some polymeric materials are reported in Table 2 below. The maximum pore size to prevent wetting should be between 0.1–0.6 μm [33,34]. Moreover, the possibility of liquid penetration in VMD is higher than other MD configurations, so a small pore size is recommended [10,35].

3.2. Membrane thickness

The membrane thickness is a significant characteristic in the MD system. There is an inversely proportional relationship between the membrane thickness and the permeate flux. The permeate flux is reduced as the membrane becomes thicker, because the mass transfer

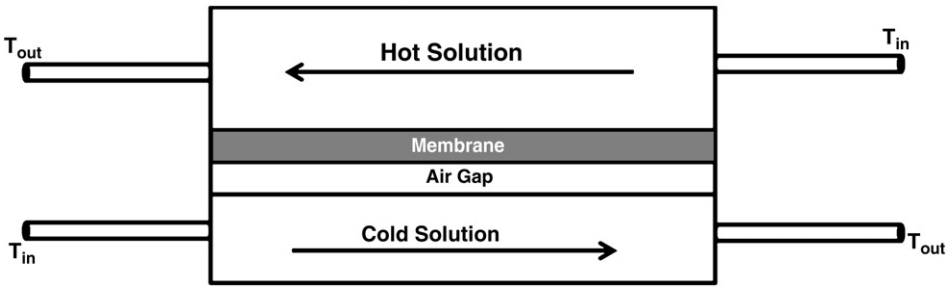

Fig. 3. Air Gap Membrane Distillation (AGMD).

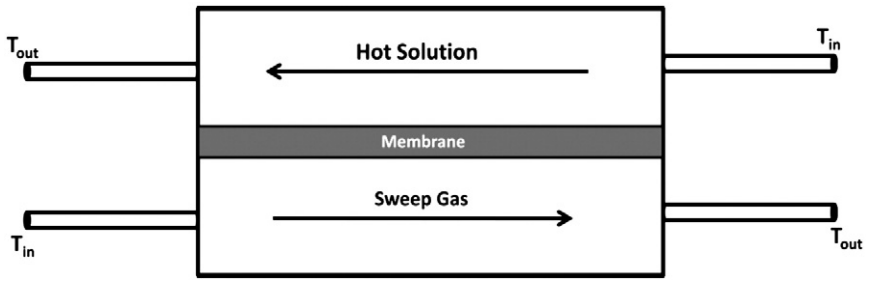

Fig. 4. Sweeping Gas Membrane Distillation (SGMD).

resistance increases, while heat loss is also reduced as the membrane thickness increases. Membrane morphology, such as thickness and pore size distribution, has been studied theoretically by Lagana et al. [38]. They concluded that the optimum membrane thickness lies between 30–60 μm. It is worth noting that the effect of membrane thickness in AGMD can be neglected, because the stagnant air gap represents the predominant resistance to mass transfer.

3.3. Membrane porosity and tortuosity

Membrane porosity refers to the void volume fraction of the membrane (defined as the volume of the pores divided by the total volume of the membrane). Higher porosity membranes have a larger evaporation surface area. Two types of liquid are used to estimate membrane porosity. The first penetrates the membrane pores (e.g. isopropyl alcohol, IPA), while the other, like water, does not. In general, a membrane with high porosity has higher permeate flux and lower conductive heat loss. The porosity (ε) can be determined by the Smolder–Franken equation [39]

$$\varepsilon = 1 - \frac{\rho_m}{\rho_{pol}} \tag{3}$$

where ρ_m and ρ_{pol} are the densities of membrane and polymer material, respectively.

According to El-Bourawi et al. [40], membrane porosity in the MD system varies from 30 to 85%.

Tortuosity (τ) is the deviation of the pore structure from the cylindrical shape. As a result, the higher the tortuosity value, the lower the permeate flux. The most successful correlation was suggested by Macki–Meares [41], where:

$$\tau = \frac{(2-\varepsilon)^2}{\varepsilon} \tag{4}$$

3.4. Mean pore size and pore size distribution

Membranes with pore size between 100 nm to 1 μm are usually used in MD systems [10,40]. The permeate flux increases with increasing membrane pore size [40]. The mechanism of mass transfer can be determined, and the permeate flux calculated, based on the membrane pore size and the mean free path through the membrane pores taken by transferred molecules (water vapour). Generally, the mean pore size is used to determine the vapour flux. A large pore size is required for high permeate flux, while the pore size should be small to avoid liquid penetration. As a result, the optimum pore size should be determined for each feed solution and operating condition.

In fact, the membrane does not have a uniform pore size so more than mass transfer mechanisms occur simultaneously (depending to the pore size). There are several investigations examine the importance of pore size distribution in MD flux [42–46]. Khayet et al [43] reported that, care must be taken when mean pore size is utilized to calculate vapour transfer coefficient instead of pore size distribution. However, Martinez et al [45] obtained a similar vapour transfer coefficient when the mean pore size and pore size distribution were used. Better understanding of membrane morphology such as pore size, pore size distribution, porosity, and thickness directs to have an accurate mass and heat transfer modelling. Regarding to the MD membrane, two types of characteristics can be analysed, the structural characteristic and the actual separation parameters (permeation) [36,37,40,47].

3.4.1. Scanning Electron Microscopy (SEM)

The top surface (i.e. the geometry of the pores), the cross-section and the bottom surface can be studied using Scanning Electron Microscopy (SEM). In addition, SEM is able to estimate the surface porosity, pore size and pore size distribution as shown in micrographs.Khemakhem and Ben Amar [29] used SEM to study the morphology, surface quality and thickness for the top layer of hydrophobic ceramic membrane. Moreover, Khayet et al [47] analysed the structure of porous membrane by SEM. The principle of SEM can be summarized in that a narrow beam of electrons with high energy hits the atoms on the surface of the sample. As a result, low energy electrons are liberated from the sample, which determines the micrograph image. Consequently, the sample should be coated (with a thin gold layer) to protect the surface.

3.4.2. Atomic Force Microscopy (AFM)

Atomic Force Microscopy (AFM) is used to determine the surface morphology of MD membrane. For example, Khayet et al [35,47] obtained A 3-dimensional image for PVDF membrane surface without

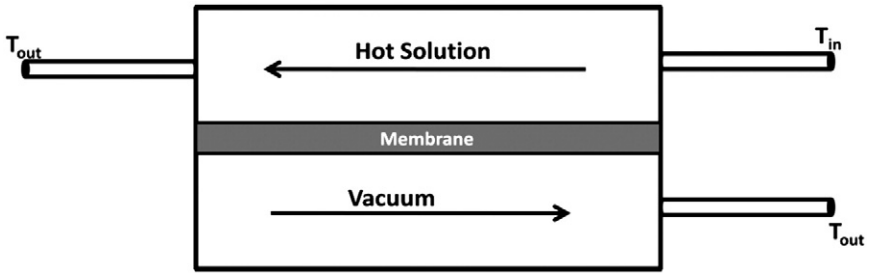

Fig. 5. Vacuum Membrane Distillation (VMD).

Table 1
Commercial flat sheet membrane commonly used in MD (modified) [36].

Trade name	Manufacturer	Material	Mean pore size (μm)	LEP_W (kPa)
TF200	Gelman	PTFE/PP[a]	0.20	282
TF450	Gelman	PTFE/PP	0.45	138
TF1000	Gelman	PTFE/PP	1.00	48
GVHP	Millipore	PVDF[b]	0.22	204
HVHP	Millipore	PVDF	0.45	105[c]
FGLP	Millipore	PTFE/PE[a]	0.20	280
FHLP	Millipore	PTFE/PE	0.50	124
Gore	Millipore	PTFE	0.20	368[c]
Gore	Millipore	PTFE	0.45	288[c]
Gore	Millipore	PRFE/PP[a]	0.20	463[c]

LEP_W: membrane liquid entry pressure of water.
[a] Polytetrafluoroethylene (PTFE) supported by polypropylene (PP) or polyethylene (PE).
[b] Polyvinylidene fluoride membrane.
[c] Measured value.

sample pre-treatment at ambient temperature and pressure. The pore size, porosity, pore size distribution and roughness parameter were determined by using this technique.

3.4.3. Bubble point with gas permeation (wet and dry flow method)

The wet and dry flow method can be applied to measure the maximum and mean pore sizes, as well as the pore size distribution of the membrane. This technique was used by Khayet and Matsuura [48] to determine the mean pore size and pore size distribution of a PVDF flat sheet membrane. The method can be summarized in that gas permeation is measured for a dry membrane at different applied pressures; a straight line relationship is obtained between the gas permeation and pressure difference. The membrane is then wetted by a liquid with low surface tension, like isopropyl alcohol (IPA), and again the gas flow is measured as a function of applied pressure. Initially, all the membrane pores are filled with IPA, and so at very low applied pressure, the pores remain filled with IPA. By increasing the applied pressure, the largest pores will be emptied of liquid, and the gas flux starts to increase. The applied pressure is steadily increased until all pores are empty, and the gas flux equals that of the gas flux through the dry membrane. A non-linear graph is obtained in plotting the gas flux as a function of pressure.

3.4.4. Permeability method

Kong and Li [49] improved the gas permeation method to determine the mean pore size (d_p), effective porosity and pore size distribution. Nitrogen can be used as standard gas. The gas permeation is measured at different operating pressures. The slope and the intercept obtained from plotting the permeate flux and pressure can be used to calculate the pore size and effective porosity. The effective porosity can be defined as the ratio of the porosity (ε) to the effective pore length (L_p) [47].

3.5. Thermal conductivity

The thermal conductivity of the membrane is calculated based on the thermal conductivity of both polymer k_s and gas k_g (usually air). The thermal conductivity of the polymer depends on temperature, the degree of crystallinity, and the shape of the crystal. The thermal conductivities of most hydrophobic polymers are close to each other. For example, the thermal conductivity of PVDF, PTFE and PP at 23 °C are 0.17–0.19, 0.25–0.27 and 0.11–0.16 $Wm^{-1}K^{-1}$ respectively [50]. The thermal conductivity of PTFE can be estimated by [51]

$$k_s = 4.86\times10^{-4}\,T + 0.253 \tag{5}$$

The thermal conductivity of the MD membrane is usually taken a volume-average of both conductivities k_s and k_g as follows:

$$k_m = (1-\varepsilon)k_s + \varepsilon k_g \tag{6a}$$

However, Phattaranawik et al. [50] suggested that thermal conductivity of an MD membrane is better based on the volume-average of both resistances ($1/k_g$ and $1/k_s$), i.e.,

$$k_m = \left[\frac{\varepsilon}{k_g} + \frac{(1-\varepsilon)}{k_s}\right]^{-1} \tag{6b}$$

for, the thermal conductivity values for air and water vapour at 25 °C are of the same order of magnitude. For instance, the thermal conductivity of air at 25 °C is 0.026 $Wm^{-1}K^{-1}$ and for water vapour, it is 0.020 $Wm^{-1}K^{-1}$. As a result, the assumption of one component gas present inside the pores is justified. Jonsson et al. [52] pointed out that the thermal conductivity of water vapour and air at around 40 °C can be computed by:

$$k_g = 1.5\times10^{-3}\sqrt{T} \tag{7}$$

Khayet et al. [53] suggested some ways to reduce the heat loss by conduction through the membrane; using membrane materials with low thermal conductivities, using a high porosity membrane, using thicker membrane, and minimizing heat losses. It is also suggested that the permeability can be enhanced by using a composite porous hydrophobic/hydrophilic membrane. In this case, the top layer is very thin hydrophobic layer to stop liquid penetration, followed by thick hydrophilic layer. Both layers reduce the heat losses through the membrane. Imdakm and Matsuura [42] developed a Monte Carlo simulation model to study the vapour permeate through a composite membrane and membrane surface temperature simultaneously.

Several studies have made improvements to membrane properties. Feng et al. [54] prepared two microporous membranes, made from PVDF and a modified PVDF (polyvinyliden fluoride-co-tetrafluroethylene). The mechanical performance and hydrophobicity of the modified PVDF membrane was better than the normal PVDF membrane. The modified PVDF membrane was used successfully in Direct Contact Membrane Distillation (DCMD), where the rejection was almost 100%. Furthermore, the hydrophilic microporous membrane can be used in MD when the membrane surface is modified to become hydrophobic. For example, the surface of a cellulose acetate and cellulose nitrate (hydrophilic membrane) was modified by radiation grafting polymerization and plasma polymerization to become hydrophobic [55]. Hengl et al. [56] made two flat metallic (stainless steel) hydrophobic membranes, where silicone was deposited on the top surface. The pore size of those membranes was 2.6 and 5 μm respectively, and during 200 min, the flux was stable. Lawson et al. [57], also, studied the influence of membrane compaction on membrane permeability. They found that the flux increased by 11% compared to a non-compacted membrane.

Table 2
Surface energy of some polymers (modified) [37].

Polymer	Surface energy ($\times10^3$ N/m)
PTFE (polytetrafluoroethylene)	19.1
PVDF(polyvinylidenefluride)	30.3
PP (polypropylene)	30.0
PE (Polyethylene)	33.2

4. Membrane distillation application

Membrane distillation (MD) has many applications. Table 3 summarise some of MD application such as fresh water production, heavy metal removal and food industry. Most of current MD applications are still in the laboratory or small scale pilot plant phase. Actually, there are some pilot plants that have been recently developed to produce fresh water [17,58].

Table 3
Plate and frame module (flat sheet membranes) as used by some researchers.

Reference	MD process	Membrane type	Thickness (μm)	Pore size (μm)	Feed solution
[59]	DCMD	TF200	178	0.2	Pure water and humic acid
		PVDF	125	0.22	
[60]	DCMD	PVDF	125	–	Humic acid/NaCl
[61]	DCMD	PVDF	126	0.22	Pure water, NaCl, brackish and seawater
[12]	DCMD	PVDF	–	0.45	Apple juice
[14]	DCMD	PTFE	175	0.2	Seawater and NaCl
	AGMD			0.5	
[62]	DCMD	PTFE	60	0.1	Pure water
		PTFE	60	0.3	
		PVDE	100	0.2	
[63]	DCMD	PVDF	–	0.4	Pure water, NaCl and sugar
[64]	DCMD	PTFE	55	0.198	Olive mill wastewaters
[15]	DCMD	PVDF	140	0.11	Orange juice
[65]	DCMD	PVDF	120	0.22	Pure water, NaCl
			125	0.2	
[41]	DCMD	PVDF	125	0.22	Pure water and humic acid
[7]	DCMD	Not mentioned	120	0.25	Heavy metals waste
[66]	DCMD	PTFE	55	0.8	Pure water, NaCl, bovine plasma and bovine blood
			90		
[67]	AGMD	PTFE	–	0.2	LiBr and H_2SO_4
[18]	AGMD	PTFE	80	0.2	NaCl,H_2SO_4,NaOH,HCl and HNO_3
[22]	VMD	PTFE	–	0.2	Acetone, ethanol, isopropanol and MTBE
[23]	VMD	PTFE	60	0.2	Pure water, ethanol and degassing water
[24]	VMD	3MC	76	0.51	Pure water and ethanol
		3 MB	81	0.4	
		3MA	91	0.29	
[68,69]	SGMD	PTFE	178	0.2	NaCl
		PTFE	178	0.45	

5. Membrane modules

5.1. Plate and frame

The membrane and the spacers are layered together between two plates (e.g. flat sheet). The flat sheet membrane configuration is widely used on laboratory scale, because it is easy to clean and replace. However, the packing density, which is the ratio of membrane area to the packing volume, is low and a membrane support is required. Table 3 presents some characteristics for flat sheet membranes that were used by some researchers. As can be seen in Table 3, the flat sheet membrane is used widely in MD applications, such as desalination and water treatment.

5.2. Hollow fibre

The hollow fibre module, which has been used in MD, has thousands of hollow fibres bundled and sealed inside a shell tube. The feed solution flows through the hollow fibre and the permeate is collected on the outside of the membrane fibre (inside-outside), or the feed solution flows from outside the hollow fibres and the permeate is collected inside the hollow fibre (outside-inside) [9]. For instance, Lagana et al. [38] and Fujii et al. [70] implemented a hollow fibre module (DCMD configuration) to concentrate apple juice and alcohol respectively. Also, saline wastewater was treated successfully in a capillary polypropylene membrane [71]. The main advantages of the hollow fibre module are very high packing density and low energy consumption. On the other hand, it has high tendency to fouling and is difficult to clean and maintain.

It is worth mentioning that, if feed solution penetrates the membrane pores in shell and tube modules, the whole module should be changed. [9,72].

5.3. Tubular membrane

In this sort of modules, the membrane is tube-shaped and inserted between two cylindrical chambers (hot and cold fluid chambers). In the commercial field, the tubular module is more attractive, because it has low tendency to fouling, easy to clean and has a high effective area. However, the packing density of this module is low and it has a high operating cost. Tubular membranes are also utilized in MD. Tubular ceramic membranes were employed in three MD configurations: DCMD, AGMD and VMD to treat NaCl aqueous solution, where salt rejection was more than 99% [30].

5.4. Spiral wound membrane

In this type, flat sheet membrane and spacers are enveloped and rolled around a perforated central collection tube. The feed moves across the membrane surface in an axial direction, while the permeate flows radially to the centre and exits through the collection tube. The spiral wound membrane has good packing density, average tendency to fouling and acceptable energy consumption.

It is worth stating that there are two possibilities for flow in a microfiltration system; cross flow and dead-end flow. For cross flow, which is used in MD, the feed solution is pumped tangentially to the membrane. The permeate passes through the membrane, while the feed is recirculated. However, all the feed passes through the membrane in the dead-end type. [72].

6. Mechanism

Fig. 6

6.1. Mass transfer

6.1.1. Direct Contact Membrane Distillation (DCMD)

The mass flux (J) in this case is assumed to be proportional to the vapour pressure difference across the membrane, and is given by:

$$J = C_m\,[P_2 - P_3] \tag{8}$$

where C_m is the membrane coefficient, P_f and P_p are the vapour pressure at the membrane feed and permeat surfaces, which can found

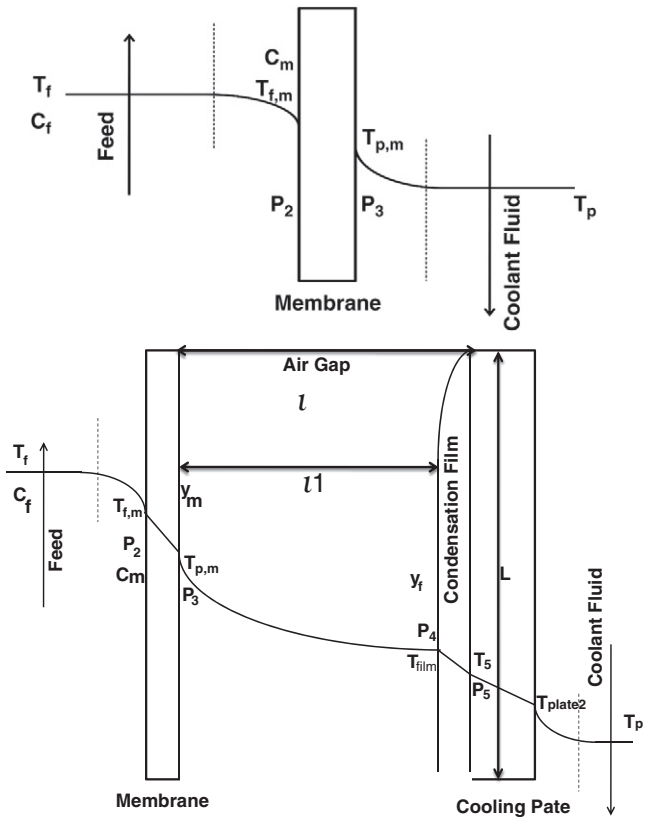

Fig. 6. Direct contact and air gap membrane distillation.

from the Antoine equation [33,67,73,74]. Therefore, Eq. (8) can be rewritten in terms of temperature difference across the membrane surfaces when the separation process is for pure water or very diluted solution, and the temperature difference across the membrane surfaces is less than or equal to 10 °C [6,10,14,43]. Hence:

$$J = C_m \frac{dP}{dT}\left(T_{f,m} - T_{p,m}\right). \tag{9}$$

The vapour pressure and temperature relationship can be expressed by the Clausius-Clapeyron equation, as follows:

$$\frac{dP}{dT} = \left[\frac{\Delta H_v}{RT^2}\right] P_0(T) \tag{10}$$

However, Schofied et al. [75] adapted Eq. (9) for more concentrated solutions, such that:

$$J = C_m \frac{dP}{dT}\left[\left(T_{f,m} - T_{p,m}\right) - \Delta T_{th}\right](1 - x_m) \tag{11}$$

where ΔT_{th} is the threshold temperature, given by:

$$\Delta T_{th} = \frac{RT^2}{M_w \Delta H_v} \frac{x_{f,m} - x_{p,m}}{1 - x_m} \tag{12}$$

where $x_{f,m}$, $x_{p,m}$, x_m, represent the mole fraction of dissolved species at the hot membrane surface side, from the permeate membrane surface side and inside the membrane, and R *and* ΔH_v represent the universal gas constant and the latent heat of vaporisation respectively.

For low concentration solution, Antoine equation can be utilized to determine the vapour pressure, because it can be assumed that the vapour pressure is a function of temperature only, i.e., dropping vapour pressure dependence on solution concentration. Martinez and Maroto [76] and Godino et al. [77] estimated the effect of both concentration and temperature on the vapour pressures by considering the water activity at the feed and permeate sides, such that:

$$P(T,x) = P_0(T) a_w(T,x) \tag{13}$$

where, $a_w(T,x)$ is water activity as a function of temperature and concentration, and $P_0(T)$ is vapour pressure of pure water at a given temperature. Raoult's law has also been used to estimate the vapour pressure [15,19], where:

$$P(T,x) = P_0(T)(1 - x) \tag{14}$$

Mass transfer through the membrane can be divided into three models. These models relate the mass transport with collisions between molecules, and/or molecules with membrane. Zhongwei et al. [62] proposed that Knudsen diffusion takes place when the pore size is too small, such that the collision between the molecules and the inside walls of the membrane suitably expresses the mass transport and the collision between molecules can be ignored. Molecular diffusion occurs when the molecules move corresponding to each other under the influence of concentration gradients. In Poiseuille flow (viscous flow), the gas molecules act as a continuous fluid driven by a pressure gradient. The Knudsen number (Kn), defined as the ratio of the mean free path (λ) of transported molecules to the membrane pore size, provides a guideline of which mechanism is active inside the membrane pore. According to kinetic theory of gases, the molecules are assumed to be hard spheres with diameter d_e and are involved in binary collisions only. It is worth noting that the collision diameter for water vapour and air are about 2.64×10^{-10}, and 3.66×10^{-10}, respectively [51]. The average distance travelled by molecules to make collisions (λ) is defined as.

$$\lambda = \frac{k_B T}{\sqrt{2}\,\pi\, P\, {d_e}^2} \tag{15}$$

k_B, T *and* P are Boltzman constant, absolute temperature, and average pressure within the membrane pores respectively. The mean free path value of water vapour at 60 °C was estimated by Al-obidni et al. [78] to be 0.11 μm.

For Kn>1 or d_p<λ (Knudsen region), the mean free path of water vapour molecules is large compared to the membrane pore size, which means the molecule-pore wall collisions are dominant over molecule-molecule collision. The mass transfer is reported by Khayet et al. [43], such that:

$$C_{Kn} = \frac{2\pi}{3} \frac{1}{RT} \left(\frac{8RT}{\pi M_w}\right)^{1/2} \frac{r^3}{\tau\delta} \tag{16}$$

where ε, τ, r, δ *and* M_w are porosity, pore tortuosity, pore radius, membrane thickness and molecular weight of water vapour, respectively.

If the k_n<0.01 or d_p>100 λ (continuum region), ordinary molecular diffusion model represents the diffusion of the vapour flux through stationary air film (the air which exist inside the membrane pores), ordinary molecular diffusion is used to describe the mass transport

$$C_D = \frac{\pi}{RT} \frac{PD}{P_{air}} \frac{r^2}{\tau\delta} \tag{17}$$

where P_{air} is the air pressure within the membrane pore, D is diffusion coefficient, and P is the total pressure inside the pore which is equal to the partial pressure of air and water vapour.

In addition, Schofield et al. [79] presented the flux of water vapour molecules, which diffuse through the membrane pores (stagnant air), as:

$$J = \frac{1}{P_{air}} \frac{\varepsilon}{\tau\delta} \frac{D\, P\, M_w}{RT} \Delta P \tag{18}$$

where P_{air} and P are the average air pressure and average gas pressure within the membrane respectively.

Removing the stagnant air existing inside the pores by degassing the feed and permeate will reduce the molecular diffusion resistance, so the membrane permeability will increase [10].

However, If $0.01<k_n<1$ or $\lambda<d_p<100\,\lambda$ (transition region), the water vapour molecules collide with each other, and also diffuse through the air film. Consequently, the mass transfer takes place by both the Knudsen/ordinary diffusion mechanism [43], where:

$$C_c = \frac{\pi}{RT}\frac{1}{\tau\delta}\left[\left(\frac{2}{3}\left(\frac{8RT}{\pi M_w}\right)^{\frac{1}{2}} r^3\right)^{-1} + \left(\frac{PD}{P_a}\, r^2\right)^{-1}\right]^{-1} \tag{19}$$

The diffusivity of water vapour through the stagnant air inside the pores is given by [44]

$$PD = 1.895\times10^{-5}\, T^{2.072} \tag{20}$$

In addition, the Fuller equation, which is a common equation to predict binary gas diffusion, can be used [80,81]

$$D = 1\times10^{-7}\frac{T^{1.75}\left(\frac{1}{Mw_a}+\frac{1}{Mw_b}\right)^{\frac{1}{2}}}{P\left[\left(\sum v_a\right)^{\frac{1}{3}}+\left(\sum v_b\right)^{\frac{1}{3}}\right]^2} \tag{21}$$

where $\sum v$ represents the diffusion volume, T is temperature in Kelvin and P is pressure in atmospheres. The diffusion volume of air and water are 20.1 and 12.7 respectively.

Lawson and Lloyd [10] stated that the molecule-pore wall collisions (Knudsen diffusion) and molecule-molecule collisions (molecular diffusion) takes place simultaneously for pore size less than 0.5 μm. Moreover, Guijt et al. [82] point out that the flux can be expressed by molecular diffusion only for large pores. Furthermore, Schofield et al. [83] and Fane et al. [84] suggested that, the vapour flux across the membrane can be expressed by Knudsen diffusion and Poiseuille (viscous) flow model for de-aerated DCMD. On the other hand, Zhongwei et al. [62] studied the effect of the Poiseuille flow mechanism in mass transfer through the membrane. They found that the Poiseuille flow should be considered as one of the mechanisms of mass transfer model in large pore size membrane.

Martinez and Maroto [76] described the transport resistance of feed, membrane and permeate resistances for pure water, NaCl and sucrose in DCMD. They concluded that it is helpful to analyse the transport in terms of resistances, to identify the controlling role of each transport step, and as a result the flux permeate can be improved. Table 4 shows DCMD membrane coefficients as reported by some researchers.

Khayet et al. [53] believed that when the pore size is near the mean free path value (critical pore size), the permeate flux under the Knudsen mechanism is higher than that obtained from the combination of Knudsen and molecular diffusion mechanisms. Therefore, choosing membranes that have small pore size may be better than membranes having large pore size. It is worth mentioning that Martinez et al. [45] studied the influence of pore size distribution in DCMD, and concluded that the effect of pore size distribution can be neglected for large pore size.

Table 4
DCMD membrane coefficient according to some researchers.

Ref	Membrane type	Pore size (μm)	Membrane coefficient (Kg/m^2 pa s)	Feed solution
[26]	PTFE	0.2	14.5×10^{-7}	Distilled water
		0.45	21.5×10^{-7}	
[46]	PVDF	0.22	3.8×10^{-7}	Distilled water
[7]	Enka (pp)	0.1	4.5×10^{-7}	Distilled water
	Enka (pp)	0.2	4.3×10^{-7}	
	PVDF	0.45	4.8×10^{-7}	
[45]	GVHP	0.22	4.919×10^{-7}	Distilled water
	HVHP	0.45	6.613×10^{-7}	

There have been several studies to investigate the influence of high concentration on the permeate flux. Martinez [85] referred the reduction of the permeate flux to the decrease in water activity. Moreover, the boundary layer solution at the membrane surface reaches saturation, so the property will vary from the bulk solution. Accordingly, Gekas and Hallstrom [86] suggested introducing the Schmidt number correction factor when a high concentration gradient occurs between the bulk and the boundary layer. Yun et al. [65], Tun et al. [87] and Schofield et al. [79] proposed that the membrane fouling resistance should also be considered.

A three dimensional Monte Carlo simulation model has been developed to study the vapour permeate through porous membrane based on kinetic gas theory and the boundary conditions that may affect the MD process [46].

6.1.2. Air Gap Membrane Distillation (AGMD)

The molecular diffusion theory is used to describe the transfer of vapour molecules through the membrane and the air gap. A stagnant gas film (air) is assumed to lie inside the membrane at the air gap side.

Kurokawa et al. [67] computed the flux by considering the diffusion in one direction through both membrane and air gap, where the air gap is below 5 mm:

$$J = \frac{P\,M_w}{RT\,P^*}\left(\frac{D}{\frac{\delta}{\varepsilon^{3.6}}+l}\right)\Delta P \tag{22}$$

where ΔP is the water vapour pressure difference between the feed on the membrane and the condensation surface, and P^* is the partial pressure of water.

Liu et al. [88] estimated the permeate flux for aqueous solution when the average operating temperature, T_a, was between 30 °C and 80 °C, thus:

$$J = \frac{T_f - T_p}{\alpha\, T_a^{-2.1} + \beta} \tag{23}$$

where α and β are parameters that can be determined experimentally.

It is worthwhile stating that the air gap is about 10 to 100 times the membrane thickness, so the effect of air inside the membrane can be neglected [10,52].

Lior and Alklaibi [89] represented the temperature, the concentration and the velocity distribution at both hot and cold channels in the two dimensional model. The temperature profile across the air gap and the effects of hot and cold temperatures on the permeate flux and process thermal efficiency were described. Furthermore, Cheryshov et al. [90] built up a mathematical model to describe the concentration distribution, velocity and temperature of salt solution in the feed channel by considering the hydrodynamics and heat transport concepts too.

Stefan diffusion was used to describe the diffusion through a stagnant gas film. It can be represented mathematically as [91]

$$N = -\frac{c\,D}{1-y}\frac{dy}{dz} \tag{24}$$

where *D*, *y*, *c and z* are diffusion coefficient, mole fraction of the vapour phase, molar concentration and diffusion length, respectively.

The Stefan equation was solved by Kimura and Nakad [18]

$$N = \frac{c\,D}{z} ln\frac{1-y_f}{1-y_m} \tag{25}$$

where y_m *and* y_f represent the mole fraction of vapour at the membrane and the condensation film, respectively.

However, Jonson et al. [52] solved the same equation by neglecting the effect of temperature and concentration polarization. They suggested that, the value of *c D* for water vapour and air at around 40 °C to be calculated using this equation:

$$c\,D = 6.3\times10^{-5}\sqrt{T} \tag{26}$$

In addition, the molar concentration can be calculated from ideal gas law:

$$c = \frac{P}{RT} \tag{27}$$

According to the standard condition, the diffusion coefficient can be corrected to the desired temperature [91] by:

$$\frac{D}{D_0} = \left[\frac{T}{T_0}\right]^{\frac{3}{2}} \tag{28}$$

Bouguecha et al. [92] used Stefan diffusion to express the vapour flux when it is governed by diffusion through the membrane pores and by natural convection through the air gap:

$$N = \frac{K_T}{R}\left[P_{f,m} - P_{film}\right] \tag{29}$$

where K_T is the overall mass transfer coefficient. Stefan diffusion was also utilized to evaluate the molar flux of seawater [5] as:

$$N = \frac{DP}{RT\,l\,P_{lm}}(P_2 - P_4) \tag{30}$$

where, P_2, P_4, D_w *and* P_{lm} are the vapour pressures at $T_{f,\,m}$, the vapour pressures at T_{film}, diffusion coefficient and log mean partial pressure respectively. The log mean partial pressure difference at the air gap is defined as:

$$P_{lm} = \frac{P_4 - P_2}{\ln\frac{P_4}{P_2}} \tag{31}$$

For a multi-component mixture, the Stefan-Maxwell equation was applied by Gostoli and Sarti [25] to express the ethanol and water vapour diffusion in stagnant gas (air). This was given by:

$$\frac{dy_i}{dz} = \sum_{j=1}^{n}\frac{1}{cD_{ij}}\left(y_iN_j - y_jN_i\right) \tag{32}$$

The vapour composition at evaporation and condensation interfaces can be calculated by assuming liquid-vapour equilibrium, such that:

$$y_i = \frac{x_i a_i P_0}{P} \tag{33}$$

Vapour pressure P_0 can be computed by the Antoine equation at the temperature of interest. The activity coefficient a_i can be calculated by the Van Laar equation at the temperature and composition of interest. The condensate composition x_i is determined by the components flux

$$x_i = \frac{N_i}{\sum N} \tag{34}$$

On the other hand, Banat and Simandl [19] employed Stefan diffusion (Eq. (24)) to represent the molar diffusion flux of an ethanol-water solution. The molar diffusion flux of ethanol and water through stagnant gas (air) in terms of pressure is given by:

$$N_i = \frac{\varepsilon D_i P}{RT\,l\,P_{lm}}(P_{i\,2} - P_{i\,4}) \tag{35}$$

For the non-equilibrium thermodynamics case, the ordinary diffusion, which is related to the concentration gradient, and thermal diffusion which is related to the temperature gradient were considered to calculate the total mass flux. A linear relation between flux and vapour pressure can be assumed, and the thermal diffusion can be neglected [33].

The Stefan–Maxwell model is reported to be more accurate than the molecular diffusion model (Fick's law) for separation of azeotropic mixtures [93,94].

6.1.3. Vacuum Membrane Distillation (VMD)

In order to remove air trapped in the membrane pores, the deaeration of the feed solution or a continuous vacuum in the permeate side should be applied. Consequently, the ordinary molecular diffusion resistance is neglected. The Knudsen mechanism is used to express the mass transfer [22,23,95,96], Poisseille flow [48] or both together [24,33,48]

For example, when the ratio of the pore radius to the mean free path $\frac{r}{\lambda}$ is <0.05, the molecule-pore wall collisions control the gas transport mechanism (Knudsen flow model) and the molar flow rate is:

$$N_i = \frac{2\pi}{3}\frac{1}{RT}\left(\frac{8RT}{\pi M_{w_i}}\right)^{\frac{1}{2}}\frac{r^3}{\delta\tau}\Delta P_i \tag{36}$$

If r is between 0.05λ and 50λ, both molecular-molecular and molecular-wall collisions should be considered. The total mass transfer is described by the Knudsen-viscous model and can be represented by the following equation:

$$N_i = \frac{\pi}{RT\delta\tau}\left[\frac{2}{3}\left(\frac{8RT}{\pi M_{w_i}}\right)^{\frac{1}{2}}r^3 + \frac{r^4}{8\mu_i}P_{avg}\right]\Delta P_i \tag{37}$$

where μ_i is the viscosity of species *i*, and P_{avg} is the average pressure in the pore.

When $\frac{r}{\lambda}$ is >50, molecular- molecular collision dominates and the mass transfer can be expressed by Poisseuille flow (viscous), such that:

$$N_i = \frac{\pi r^4}{8\mu_i}\frac{P_{avg}}{RT}\frac{1}{\tau\delta}\Delta P_i \tag{38}$$

6.1.4. Sweeping Gas Membrane Distillation (SGMD)

Khayet [36] points out that the equations, which illustrate the mass transfer of DCMD can be used in SGMD. A theoretical model was designed to predict the SGMD flux and temperature profiles in the system for two PTFE membranes. Knudsen/molecular diffusion can be used to describe the mass transfer through the membrane pores. Moreover, the circulation velocity and feed temperature are significant parameters [68,69].

Sherwood correlation can be used to estimate the mass transfer coefficient, *k*, across the boundary layers, then the concentration at the boundary layer can be evaluated. The empirical form of the Sherwood correlation is

$$Sh = \frac{k\,d}{D} = (Constant)Re^aSc^b \tag{39}$$

where *Re,Sc, and D* are Reynolds number, Schmidt number and diffusion coefficient respectively (Table 5).

Table 5
Sherwood correlations as used by some researchers.

Ref	Equation	Notes
[5,65]	$Sh = 1.86\left(Re\,Sc\frac{d}{L}\right)^{\frac{1}{3}}$	Laminar flow
[96,97]	$Sh = 1.62\left(Re\,Sc\,\frac{d_h}{L}\right)^{0.33}$	Laminar flow
[98]	$Sh = 2.00\,Re^{0.483}Sc^{\frac{1}{3}}$	Does not mention
[5,48,65,67,86]	$Sh = 0.023\,Re^{0.8}\,Sc^{\frac{1}{3}}$	Turbulent flow
[86]	$Sh = 0.023\,Re^{0.875}\,Sc^{0.25}$	Turbulent flow
[67]	$Sh = \frac{c}{\left(\frac{L}{l}\right)^{\frac{1}{9}}}(Sc\,Gr)^{n}$ $2.1\times10^{5}<Gr<1.1\times0^{7}$ $c=0.07\ n=1/3$ $2.0\times10^{4}<Gr<2.1\times10^{5}$ $c=0.20\ n=1/4$	To compute mass transfer coefficient across the air gap when it is over 5 mm

Schmidt numbers can be calculated by:

$$Sc = \frac{\mu}{\rho D} \tag{40}$$

where μ is the viscosity. For a non-circular channel, these correlations can be utilized if the equivalent (hydraulic) diameter d_{eq} is employed.

$$d_{eq} = 4r_H = 4\,\frac{S}{L_P} \tag{41}$$

where r_H, S *and* L_P are the hydraulic radius, cross sectional area of the flow channel, and length of wetted perimeter of the flow channel, respectively.

6.2. Heat transfer

Membrane distillation (MD) is a non-isothermal process. Two main heat transfer mechanisms occur in the MD system: latent heat and conduction heat transfer (see Fig. 7).

The heat transfer, which occurs in DCMD, can be divided into three regions (Fig. 7) [9,14,40,41,61,62,65,75,76,97,99–103]:

Heat transfer by convection in the feed boundary layer:

$$Q_f = h_f\left(T_f - T_{f,m}\right) \tag{42}$$

Heat transfer through the membrane by conduction, and by movement of vapour across the membrane (latent heat of vaporization). The influence of mass transfer on the heat transfer can be ignored [40,84,101–104]

$$Q_m = \frac{k_m}{\delta}\left(T_{f,m} - T_{p,m}\right) + J\Delta H_v \tag{43}$$

$$Q_m = h_m\left(T_{f,m} - T_{p,m}\right) + J\Delta H_v \tag{44}$$

where h_m represents the heat transfer coefficient of the membrane.

It is worth mentioning that h_m can be rewritten for pure water or very diluted solution, and where temperature difference across the membrane surfaces is less than or equal to 10 °C by substituting Eqs. (9) into (43)[15,75,84]:

$$Q_m = \frac{k_m}{\delta}\left(T_{f,m} - T_{p,m}\right) + \left[C_m\frac{dP}{dT}\left(T_{f,m} - T_{p,m}\right)\right]\Delta H_v \tag{45}$$

$$Q_m = \left[\frac{k_m}{\delta} + \left(C_m\frac{dP}{dT}\right)\Delta H_v\right]\left(T_{f,m} - T_{p,m}\right) \tag{46}$$

$$Q_m = h_m\left(T_{f,m} - T_{p,m}\right) \tag{47}$$

For a non-linear temperature distribution assumption, Q_m (for the x-dimension) is also expressed as [20,50,61,65,102,104]:

$$Q_m = -k_m\frac{dT}{dx} + J\Delta H_v \tag{48}$$

For the permeate side, the convection heat transfer takes place in the permeate boundary layer

$$Q_p = h_p\left(T_{p,m} - T_p\right) \tag{49}$$

At steady state, the overall heat transfer flux through the membrane is given by:

$$Q = Q_f = Q_m = Q_p \tag{50}$$

$$h_f\left(T_f - T_{f,m}\right) = \frac{k_m}{\delta}\left(T_{f,m} - T_{p,m}\right) + J\Delta H_v = h_p\left(T_{p,m} - T_p\right) \tag{51}$$

$$Q = U\left(T_f - T_p\right) \tag{52}$$

where U represents the overall heat transfer coefficient.

It is worth pointing out that the heat conduction can be neglected for non-sported thin membrane [102] and for high operating temperature as well [84,102]. Moreover, the heat transfer by convection is ignored in the MD process, except in AGMD [9].

The surface temperature of both sides of membrane cannot be measured experimentally, or calculated directly. Therefore, a mathematical iterative model has been designed to estimate these temperatures [61]:

$$T_{f,m} = T_f - \frac{J\,\Delta H_v + \frac{k_m\left(T_{f,m} - T_{p,m}\right)}{\delta_m}}{h_f} \tag{53}$$

$$T_{p,m} = T_p - \frac{J\,\Delta H_v + \frac{k_m\left(T_{f,m} - T_{p,m}\right)}{\delta_m}}{h_p} \tag{54}$$

The value of H_v should be evaluated at average membrane temperature. However, Phattarnawik and Jiaratananon [102] evaluated at logarithmic average membrane temperature.

The surface membrane temperature in terms of temperature polarisation coefficient, ψ, for pure water and very diluted solution, [75,84,99,105]

$$T_{f,m} - T_{p,m} = \frac{1}{1 + \frac{H}{h_f} + \frac{H}{h_p}}\left(T_f - T_p\right) = \psi\left(T_f - T_p\right) \tag{55}$$

where h_m is equal to

$$h_m = \left(C_m\frac{dP}{dT}\right)\Delta H_v + \frac{k_m}{\delta} \tag{56}$$

Lawson and Lloyd [10] pointed out that the $(T_{m,\,f} - T_{m,p})$ is about 0.1 °C at low flux and does not exceed 0.5 °C at high flux.

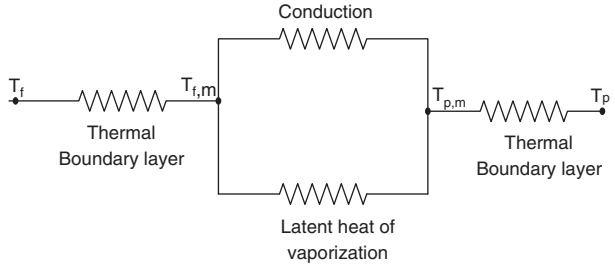

Fig. 7. Heat transfer resistances in the MD system.

Gryta et al. [106] studied the presence of free and force convection in laminar flow in DCMD, and suggested the following equation to calculate the heat transfer coefficient:

$$Nu = 0.74\, Re^{0.2} (Gr\, Pr)^{0.1}\, Pr^{0.2} \tag{57}$$

A mathematical model was built by Chen et al. [107] to study the temperature distribution on both membrane surfaces in the hot and cold membrane chambers. This model was able to compute the power consumption of DCMD.

For the AGMD configuration, the heat transfer through the AGMD was represented as in DCMD, except for the heat transfer across the air gap, which occurs by conduction and vapour (mass transfer) [6,88,108]

$$\begin{aligned} h_f\left(T_f - T_{f,m}\right) &= J\Delta H_v + \frac{k_m}{\delta}\left(T_{f,m} - T_{p,m}\right) = J\Delta H_v + \frac{k_g}{l}\left(T_{p,m} - T_{film}\right) \\ &= h_d\left(T_{film} - T_5\right) \end{aligned} \tag{58}$$

In addition, Guijt et al. [82], Banat and Simandl [19] and Kimura et al. [18] suggested the following equation to calculate the heat transfer coefficient for the condensate film (pure vapour) on a vertical wall:

$$h_d = \frac{2}{3}\sqrt{2}\left(\frac{{k_{film}}^3 \rho^2 g \Delta H_v}{\mu L\left(T_{film} - T_5\right)}\right)^{\frac{1}{4}} \tag{59}$$

Furthermore, the average membrane temperature was used by Kimura and Nakao [18] instead of membrane surface temperature. They concluded that the sensible heat for the MD system can be neglected, because it has a very small magnitude compared to the heat of vaporization

$$Q = J\Delta H_v \tag{60}$$

Free convection heat transfer between two vertical plates is also used to describe the heat transfer phenomenon in the air gap region, when the air gap distance is over 5 mm [67]

$$Nu = c\,(\mathrm{Pr}\, Gr)^n \left(\frac{l}{L}\right)^{\frac{1}{9}} \tag{61}$$

where

$$10^5 < Gr < 10^7,\ c = 0.07\ and\ n = \frac{1}{3}$$
$$10^4 < Gr < 10^5,\ c = 0.2\ and\ n = \frac{1}{4}$$

Bouguecha et al. [92] designed a mathematical model for laminar flow, in which the heat and mass transfer are considered. The temperature profiles at different air gap thicknesses in two dimensions are plotted. The heat transfer by convection starts to change to natural convection at 5 mm air gap thickness, and this dominates the heat transfer mechanism at a wide air gap.

For VMD configuration, heat transfer by convection in the feed boundary layer can be expressed as:

$$Q_f = h_f\left(T_f - T_{f,m}\right) \tag{62}$$

However, the heat transfer by conduction through the membrane is ignored [10,35], so the heat transfer across the VMD can be written as:

$$h_f\left(T_f - T_{f,m}\right) = J\Delta H_v \tag{63}$$

For SGMD, the heat transfer equations, which describe the DCMD can be used [36].

The heat transfer coefficients of the boundary layers can be estimated by the Nusselt correlation (see Table 6). Its empirical form is:

$$Nu = Constant\, Re^a Pr^b \tag{64}$$

Consequently, the heat transfer coefficient h can be calculated using Reynolds and Prandtl numbers(*Re and Pr*), i.e.

$$\text{Reynolds number} = R_e = \frac{v\, d\, \rho}{\mu} \tag{65}$$

$$\text{Prandtl number} = Pr = \frac{c_p\, \mu}{k} \tag{66}$$

$$\text{Grashoff number} = G_r = \frac{g\, \beta \Delta T L^3\, \rho^2}{\mu^3} \tag{67}$$

where v, ρ, μ, c_p, g, β, L *and* k are fluid velocity, density, viscosity, heat capacity, gravity acceleration, thermal expansion coefficient, height and thermal conductivity.

The mass transfer and the heat transfer can be related, as proposed by Garcia-Payo et al. [6] by:

$$Sh\, Sc^{\frac{-1}{3}} = Nu\, Pr^{\frac{-1}{3}} \tag{68}$$

7. Thermal efficiency and energy consumption

The thermal efficiency Π in MD can be specified as the ratio of latent heat of vaporization to the total (latent and conduction) heat. Al-obaidani et al. [78] pointed out that the thermal efficiency can be improved by increasing the feed temperature, feed flow rate and membrane thickness. In contrast, it decreases when the concentration for salt solution increases.

Table 6
Correlations used to estimate heat transfer coefficient.

Ref	Equations	Notes
[10]	$Nu = 0.023\, Re^{0.8} Pr^{\frac{1}{3}} \left(\frac{\mu}{\mu_s}\right)^{0.14}$	Turbulent flow ($2500 < Re < 1.25 \times 10^5$)
[41]	$Nu = 0.023\, Re^{0.8}\, Pr^n$ n = 0.4 for heating, n = 0.3 for cooling	Turbulent flow ($2500 < Re < 1.25 \times 10^5$) $0.6 < Pr < 100$
[43]	$Nu = 0.027\, Re^{\frac{4}{5}} Pr^n \left(\frac{\mu}{\mu s}\right)^{0.14}$ n = 0.4 for heating, n = 0.3 for cooling	Turbulent region
[50,61,44]	$Nu = 0.023\left(1 + \frac{6d}{L}\right) Re^{0.8} Pr^{\frac{1}{3}}$	The most suitable heat Transfer correlation for Turbulent flow
[50,61,44]	$Nu = 3.36 + \frac{0.036\, RePr\, \frac{d}{L}}{1 + 0.0011\left(RePr\frac{d}{L}\right)^{0.8}}$	The best correlation to Compute the heat Transfer coefficient for The laminar flow
[41,101]	$Nu = 1.86\, \left(RePr\frac{d}{L}\right)^{0.33}$	For laminar flow ($Re < 2100$) Recommended for flat sheet module
[87,109]	$Nu = 1.86\, Re^{\frac{1}{3}} Pr^{\frac{1}{3}} \left(\frac{d}{L}\right)^{\frac{1}{3}} \left(\frac{\mu}{\mu_s}\right)^{\frac{1}{7}}$	Laminar flow
[110]	$Nu = 1.86\, Re^{0.96} Pr^{\frac{1}{3}} \left(\frac{d}{L}\right)^{\frac{1}{3}}$	Laminar flow
[18]	$Nu = 1.62\left[RePr\frac{d}{L}\right]^{\frac{1}{3}}$	Laminar flow
[106]	$Nu = 0.298\, Re^{0.646} Pr^{0.316}$	Laminar flow $150 < Re < 3500$
[106]	$Nu = 0.74\, Re^{0.2} (Gr\, Pr)^{0.1}\, Pr^{0.2}$	The best correlation for plate and frame module in laminar flow
[9]	$Nu = 0.036\, Re^{0.8}\, Pr^{0.33}\, \left(\frac{d}{L}\right)^{0.055}$	Turbulent flow
[110]	$Nu = 0.036\, Re^{0.96}\, Pr^{0.33}\, \left(\frac{d}{L}\right)^{0.055}$	Turbulent flow in tube and $10 \leq \frac{L}{d} \leq 400$
[111]	$Nu = 1 + 1.44\left(1 - \frac{1708}{Re}\right) + \left[\left(\frac{Re}{5830}\right)^{\frac{1}{3}} - 1\right]$	Not mentioned

For DCMD, the thermal efficiency Π can be expressed as:

$$\Pi = \frac{J\Delta H_v}{J\Delta H_v + \frac{k_m}{\delta}\left(T_{f,m} - T_{p,m}\right)} \tag{69}$$

For pure water, Bandini et al. [112] commented that the characteristics of the membrane, such as porosity and tortuosity, determine the thermal efficiency, with no dependence on membrane thickness.

Around 50–80% of the total heat flux across the membrane is considered to be latent heat; whereas 20–40% of heat is lost by conduction through the membrane [10,84]. The heat lost by mass flux can be estimated by:

$$\frac{Q_{lost}}{J} = \frac{k_m}{C_m}\frac{\left(T_{f,m} - T_{p,m}\right)}{(P_2 - P_3)} \tag{70}$$

Martinez-Diez et al. [113] cast the above equation for a very dilute solution, and low membrane temperature difference in the following form:

$$\frac{Q_{lost}}{J} = \frac{k_m}{C_m}\frac{1}{\left(\frac{dP}{dT}\right)_{T_m}} \tag{71}$$

A least-squares method was then used to determine the heat lost by fitting the experimental points $\left(\left(\frac{dP}{dT}\right)^{-1}, \frac{Q_{lost}}{J}\right)$:

$$\frac{Q_{lost}}{J} = (0.1 \pm 0.3) + (0.56 \pm 0.05)\left(\frac{dP}{dT}\right)^{-1} \tag{72}$$

They concluded that working at a high temperature and flow rate reduces the heat loss.

Fane et al. [84] pointed out that there are three forms for heat transfer to be lost in the DCMD system. The first form is due to the presence of air within the membrane. Secondly, heat loss through the membrane by conduction, and finally by temperature polarization. They suggested some solutions to minimize heat loss in the DCMD, such as: de-aeration of the feed solution, increasing the membrane thickness, creating an air gap between the membrane and the condensation surface, and operating within a turbulent flow regime.

In terms of AGMD thermal efficiency, Liu et al. [88] suggested that the thermal efficiency is proportional to the membrane distillation temperature difference. They introduced two parameters α and β, which can be determined experimentally for an air gap less than 5 mm, and average membrane distillation temperature, T_a, between 30 °C and 80 °C by:

$$\eta = 1 - \frac{\alpha\, {T_a}^{-2.1}}{\lambda}\left(\frac{\left(T_f - T_p\right) c_p}{\alpha\, {T_a}^{-2.1} + \beta} + \frac{k_a}{l}\right) \tag{73}$$

c_p *and* k_a are specific heat and air gap thermal conductivity.

Lior and Alklaibi [89] observed that by increasing the feed temperature from 40 °C to 80 °C, the thermal efficiency increased by 12%, whereas the salt concentration has a marginal effect on the thermal efficiency.

With regard to energy consumption, Criscuoli et al. [114] used a simple energy balance to compute the energy consumption of hot and cold streams for DCMD and VMD using different flow configurations.

$$Q = \dot{m}\, cp\, \Delta T \tag{74}$$

They found that the cross-flow configuration is the best, in terms of high flux and energy consumption. Moreover, hybrid RO/MD becomes the best choice when an external energy source is available [2]. In addition, heat transfer to the cooling side by heat conduction, and by heat of condensation can be used (recovered) to preheat the feed solution, which minimizes the heat requirement and improves the operation cost. The percentage of heat recovery depends on the heat exchanger area. Schneider et al. [34] indicated that the MD performance rises by 8% when heat recovery is used. Kurokawa and Sawa [3] reported that the heat input declines with increasing heat exchanger and membrane areas. They optimized the value of both heat exchanger and membrane areas for a plate and frame cell and PTFE membrane (0.2 μm pore size); this was 0.2 m^2. Likewise, Ding et al. [115] emphasized that the heat exchanger capacity should be optimized with membrane area, in order to get high production flux for a solar powered membrane distillation system. From the economic point of view, Hogan et al. [116] observed that the capital cost is very sensitive to heat recovery, because the heat exchanger is the most expensive item in a solar-powered MD plant. They optimized solar collector area, membrane area and heat recovery to achieve low capital cost and high flux.

8. Temperature polarization and concentration polarization

Since the vaporization phenomenon occurs at the membrane hot surface and condensation at the other side of membrane, thermal boundary layers are established on both sides of the membrane. The temperature difference between the liquid-vapour interface and the bulk is called temperature polarization, ψ [61,75,84,99,105], which is defined as:

$$\psi = \frac{T_{m,f} - T_{m,p}}{T_f - T_p} \tag{75}$$

Lawson [10] represented ψ with slight difference for VMD as:

$$\psi = \frac{T_f - T_{m,f}}{T_f - T_p} \tag{76}$$

The effect of heat transfer boundary layer to total heat transfer resistance of the system is measured by temperature polarization.

When the thermal boundary layer resistances are reduced, the temperature difference between the liquid-vapour interface and the bulk temperature becomes close to each other and, consequently, ψ approaches 1, which means a typical system. On the other side, zero ψ means a high degree of concentration polarization is taking place, and the system is controlled by large boundary layer resistance. Usually, the value of ψ lies between 0.4–0.7 for DCMD [9,10,97,99,102]. Termpiyakul et al. [61] pointed out that temperature polarization becomes important at high concentration, high temperature and low feed velocity.

Concentration polarization, Φ is defined as the increase of solute concentration on the membrane surface (c_m) to the bulk solute concentration (c_f):

$$\Phi = \frac{c_m}{c_f} \tag{77}$$

In order to estimate the concentration of the solute (mole fraction) on the membrane surface, Martinez [18], Martinez and Vazquez [31] and Martinez and Maroto [111] suggested the following relation:

$$c_m = c_f\, exp\left(\frac{j}{\rho K}\right) \tag{78}$$

where ρ is the liquid density and K is mass transfer coefficient.

Yun et al. [65] studied the influence of high concentration on mass transfer coefficient and distilled flux. Pure water and high concentration of NaCl (17.76%, 24.68%) are used as feed. They found that the viscosity, density of the feed, solute diffusion coefficient, and the

convective heat transfer coefficient are directly related to the concentration and temperature. They noted that the solute accumulated on the membrane surface during the desalination process; as a consequence, a diffusive flow back to the feed was generated. Therefore, the concentration polarization and fouling must be considered in modelling, and the permeate flux cannot be predicted by Knudsen, molecular and Poiseuille flow, because the properties of the boundary layer at the membrane surface vary from the bulk solution.

9. Fouling

The fouling problem is significantly lower than that encountered in conventional pressure-driven membrane separation. Shirazi et al. [117] pointed out that membrane fouling by inorganic salt depends on the membrane properties, module geometry, feed solution characteristic and operating conditions. There are several types of fouling, which may block the membrane pores. Biological fouling is growth on the surface of the membrane (by bacteria), and scaling (for the high concentration solution), which will create an additional layer on the membrane surface, composed of the particles present in the liquid [10].

Kullab and Martin [58] pointed out that fouling and scaling lead to blocking the membrane pores, which reduces the effective membrane, and therefore the permeate flux obviously decreases. These may also cause a pressure drop, and higher temperature polarization effect. Gryta [118] indicated that the deposits formed on the membrane surface leads to the adjacent pores being filled with feed solution (partial membrane wetting). Moreover, additional thermal resistance will be created by the fouling layer, which is deposited on the membrane surface. As a result, the overall heat transfer coefficient is changed. For DCMD at steady state, Gryta [119] specified:

$$h_f\left(T_f - T_{f,foulig}\right) = \frac{k_{fouling}}{\delta_{fouling}}\left(T_{f,fouling} - T_{f,m}\right) = \frac{k_m}{\delta}\left(T_{f,m} - T_{p,m}\right) + J\Delta H_v = h_p\left(T_{p,m} - T_p\right) \quad (79)$$

where $k_{fouling}$, $\delta_{fouling}$ *and* $T_{f,\ fouling}$ are the fouling layer thermal conductivity, thickness, and fouling layer temperature, respectively.

Tun et al. [87] examined the effect of high concentration of NaCl and Na_2SO_4 on the permeate flux. The flux gradually decreases during the MD process, until the feed concentration reaches the supersaturation point, and then the flux decrease sharply to zero. Afterwards, the membrane was completely covered by crystal deposits. Furthermore, Yun et al. [65] arrived at the same result, and concluded that when the membrane surface concentration reaches saturation, the properties of the boundary layer will differ from the bulk solution properties.

Currently, pre-treatment and membrane cleaning are the main techniques to control fouling. Alklaibi and Lior [32] investigated the influence of fouling by preparing three different solutions: water pre-treated by microfiltration, seawater and 3% NaCl. They concluded that the pre-treatment process increased the product flux by 25%, which means that the pre-treatment process is important, in order to enhance the permeate flux. Hsu et al. [14] used the ultrasonic irradiation technique to clean fouling from the membrane. Moreover, pure water for 2 h, followed by 0.1 M NaOH was used to clean a membrane, which was utilized to filter a mixture of $CaCl_2$ and humic acid. The permeate flux was about 87% of initial flux [60]. Gryta [119] proposed that the fouling intensity can be limited by operating at low temperature (feed temperature), and increasing the feed flow rate.

10. Operating parameters

In this section, the influence of feed temperature, concentration and air gap will be reviewed and major findings will be cited and discussed.

10.1. Feed temperature

As can be seen in Table 7, the feed temperature has a strong influence on the distilled flux. According to the Antoine equation, the vapour pressure increases exponentially with temperature. Therefore, the operating temperature has an exponential effect on the permeate flux [32]. At constant temperature difference between the hot and the cold fluid, the permeate flux increases when the temperature of the hot fluid rises, which means the permeate flux is more dependent of the hot fluid temperature [12]. Qtaishat et al. [103], Gunko et al. [12], and Chen et al. [107] pointed out that increasing the temperature gradient between the membrane surfaces will affect the diffusion coefficient positively, which leads to increased vapour flux. Similarly, Srisurichan et al. [41] believed that there is a direct relation between diffusivity and temperature, so that working at high temperature will increase the mass transfer coefficient across the membrane. Moreover, temperature polarization decreases with increasing feed temperature [50,102]. In terms of coolant temperature, a noticeable change takes place in the permeate flux when the cold side temperature decreases [12,15]. In addition, more than double permeate flux can be achieved compared to a solution, at the same temperature difference [32]. Banat and Simandl [5] and Matheswaran et al. [120], however, found that the effect of the cold side temperature on the permeate flux is neglected at fixed hot side temperature, because of low variation of vapour pressure at low temperatures.

10.2. The concentration and solution feature

There is a significant fall in the flux product when feed concentration increases due to decreasing vapour pressure [85] and increasing

Table 7
Effect of temperature on permeate flux.

Ref	MD type	Membrane type	Pore size (μm)	Solution	Feed velocity (m/s)	T_f (°C)	Permeate kg/m^2 h
[5]	AGMD	PVDF	0.45	Artificial seawater	5.5 l/min	40–70	≈1–7
[50]	DCMD	PVDF	0.22	Pure water	0.1	40–70	≈3.6–16.2
[113]	DCMD	PTFE	0.2	NaCl (2 mol/l)	16 cm^3/s	17.5–31	≈2.88–25.2
[44]	DCMD	PTFE	0.2	Pure water	–	40–70	≈5.8–18.7
[63]	DCMD	PVDF	0.4	Sugar	0.45	61–81	≈18–38
[65]	DCMD	PVDF	0.4	Pure water	0.145	36–66	≈5.4–36
				NaCl (24.6 wt.%)	0.145	43–68	≈6.1–28.8
[24]	VND	3MC	0.51	Pure water	–	30–75	≈0.8–8.8 mol/m^{2}s
[41]	DCMD	PVDF	0.22	Pure water	0.23	40–70	≈7–33 l/m^{2}h
[68]	SGMD	PTFE	0.45	Pure water	0.15	40–70	≈4.3–16.2
[15]	DCMD	PVDF	0.11	Orange juice	2.5 kg/min	25–45	30×10^3–108×10^3
[14]	DCMD	PTFE	0.2	NaC l (5%)	3.3 l/min	5–45	1–42
[14]	AGMD	PTFE	0.2	NaC l (3%)	3.3 l/min	5–45	0.5–6

Table 8
Effect of concentration on permeate flux.

Ref	MD type	Membrane type	Pore size (μm)	Solution	Concentration g/l	T_f (°C)	Permeate kg/m^2 h
[6]	AGMD	PVDF	0.22	Methanol/water	≈30–200	50	≈ 3.9–4.6
				Ethanol/water	≈30–150		≈3.95–4.9
				Isopropanol/water	≈10–95		≈4.0–5.0
[113]	DCMD	PTFE	0.2	NaCl	0–116.8	31	≈32.4–25.2
[63]	DCMD	PVDF	0.4	NaCl	0–5290	81	≈44–63
[65]	DCMD	PVDF	0.22	NaCl	0–24.6 wt.%	68	≈36–28.8
[120]	AGMD	PTFE	0.22	HNO_3	2–6 M	80	≈0.9–2.1 l/m^{2}h
[120]	VMD	PP	0.2	NaCl	100–300	55	10.7–7.0

temperature polarization [101]. Likewise, Izquierdo-Gil et al. [108] concluded that the reduction in product flux is linear with time. Furthermore, Tomaszewska et al. [16,109] studied the influence of acid concentration on the permeate flux. They found that there is a reduction in the permeate when the acid concentration increase. Moreover, Sakia et al. [66] found a noticeable reduction in the water vapour permeability when protein concentration of bovine plasma increases. On the other hand, Banat and Simandl [33], Qtaishat et al. [103] and Alklaibi and Lior [89] concluded that the permeate flux decreases slightly with increasing feed concentration. About 12% reduction in permeate flux happened when the feed (NaCl) increased from 0 to 2 Molar concentration [103]. This decrease in the permeate flux amount is due to the reduction in the water vapour pressure. Lawson and Lloyd [10] studied the reasons for decreasing product flux when the concentration of NaCl increases. They found three reasons for this reduction; 1) water activity, which is a function of temperature, decreases when the concentration increases 2) the mass transfer coefficient of the boundary layer at the feed side decreases due to increased influence of concentration polarization, and 3) the heat transfer coefficient decreases as well at the boundary layer, because of the reduction in the surface membrane temperature. Therefore, the vapour pressure of the feed declines, which leads to reduced performance of MD. Schofield et al. [63] studied the impact of molecular weight fraction and viscosity on the flux by preparing sugar (30 wt.%) and NaCl (25 wt.%) solutions. Under the same conditions, they found that the sugar solution has less flux reduction than salt solution. They concluded that the viscosity is an important factor in flux reduction. The heat transfer coefficient decreases due to the reduced Reynolds number. The effect of thermal conductivity and heat capacity on the flux reduction is negligible. Furthermore, the impact of density on the flux production is important for salt solutions. Three aqueous solutions of methanol, ethanol and isopropanol at different concentrations were studied by Garcia et al [6]. They found that the type of alcohol is strongly related to the amount of flux. Isopropanol has the highest vapour pressure, and as a consequence isopropanol solution has the highest flux, while methanol solution has the lowest.

The influence of high concentration, such as in NaCl solutions, was reported by Yun [65], who found that there is variation in the permeate flux with time (see Table 8), and that it is difficult to calculate the permeate flux using existing models.

10.3. Recirculation rate

Table 9 summarizes the effect of recirculation rate. Working at a high recirculation rate minimizes the boundary layer resistance and maximizes the heat transfer coefficient. As a result, higher flux can be achieved [41]. Chen et al. [107] indicated that the increasing volumetric flow rate will enhance the permeate flux. The fluid velocity rises when the volumetric flow rates increases, so that the convective heat transfer coefficient develops and the thermal boundary layer thickness decreases. As a result, the temperature polarization effect reduces. Moreover, Martinez-Diez and Vazques-Gonzalez [101] found significant change in temperature polarization, when the rate of recirculation changes. This is because the recirculation rate enhances the heat transfer, which leads to rise in the product flux and temperature polarization. Izquierdo-Gil et al. [108] investigated the influence of increasing the flow rate on the flux product. The concentration and temperature polarization decreased due to the higher flow rate. Banat and Simandl [5], and Shojikubota at al. [122] studied the effect of flow rate on the cold side. Shojikubota at al. They found that the cold side flow rate has an important effect on the permeate flux; however, Banat and Simandl [5] found negligible influence on the permeate flux, when the cold side flow rate was enhanced.

10.4. The air gap

Lawson and Lloyd [10] pointed out that the flux declines linearly with $\frac{1}{l}$. Likewise, Izquierdo-Gil et al. [108] found a linear relation between the distillate flux and the number of gaskets removed. They studied the effect of opening the upper side of the gap to the atmosphere as well. A slight reduction in distillate flux happened compared to closing the gap. Alklaibi and Lior [32] reported that reducing the air gap will

Table 9
Effect of recirculation rate on permeate flux.

Ref	MD type	Membrane type	Pore size (μm)	Solution	T_f (°C)	Flowrate m/s	J (kg/m^{2}h)
[68,69]	SGMD	TF200	0.2	NaCl(1 M)	50	0.07–0.21	≈3.24–3.96
		TF450	0.45				≈5.4–5.76
[61]	DCMD	PVDF	0.22	NaCl (35 g/l)	60	1.85–2.78	31–38
[5]	AGMD	PVDF	0.45	Artificial Seawater	60	1–5.7 l/min	≈2.7
[85]	DCMD	PTFE	0.2	Sucrose (40 wt %)	39	5–16 cm^3/s	5.7–9.0
[63]	DCMD	PVDF	0.4	Sugar (30 wt %)	81	0.45–0.9	≈38–55
[65]	DCMD	PVDF	0.22	NaCl (17.7 wt %)	68	0.056–0.33	≈25.9–29.5
[24]	VMD	3MC	0.51	Pure water	74	37–63 cm^3/s	≈6.4–8.7 mol/m^{2}s
[41]	DCMD	PVDF	0.22	Pure water	50	1.8–2.3	≈18–20 l/m^{2}h
[22]	VMD	PTFE	0.2	Acetone (5 wt.%)	30	0.1–2.6 l/min	12.6–21.6
[121]	VMD	PP	0.2	NaCl (300 g/l)	55	0.015–0.03 l/s	7–9.1

Table 10
Air gap effect on the permeate flux.

Ref	Membrane type	Pore size (μm)	Solution	T_{in} °C	Air gap (mm)	Permeate kg/m^2.h
[5]	PVDF	0.45	Artificial seawater	60	1.9–9.9	≈5–2.1
[6]	PTFE	0.2	Isopropanol	50	1.62–0.55	≈5.1–6.3
[108]	PVDF	0.22	Sucrose	25.8	1–4	≈0.8–1.7 l/m^{2}h
[18]	PTFE	0.2	NaC l(3.8%)	60	0.3–9	≈19–1.5
[120]	PTFE	0.22	HNO_3 (4 M)	80	0.5–2	≈5.3–4.25 l/m^{2}h
[123]	PTFE	0.45	HCl/water	60	4–7	≈3.7–2.4
[123]	PTFE	0.2	Propionic Acid/water	60	4–7	≈7.4–4.6

double the flux product, with a more significant effect when the gap is less than 1 mm. Banat and Simandl [5] concluded that reducing the air gap width will increase the temperature gradient within the gap, which leads to increased permeate flux. Table 10 summarizes the air gap effect on the permeate flux.

10.5. Membrane type

The membrane permeation flux is proportional to the porosity, and inversely proportional to the membrane thickness and tortuosity [124]. Izquierdo-Gil et al. [108] observed that for a larger pore size membrane, higher permeate flux is obtained. In addition, higher flux is achieved using a membrane without support, compared to the same membrane pore size with support [6]. Likewise, Izquierdo-Gil et al. [108] and Alklaibi and Lior [32] concluded that for a more efficient MD process, low thermal conductivity material should be used (unsupported membrane).

10.6. Long operation

Izquierdo-Gil et al. [108] did not observe any change in distillate flux during a month of operation. On the other hand, Scheider et al. [34] reported a 20% decline in permeate flux after 18 weeks, when tap water was used in a DCMD. Lawson and Lloyd [10] suggested that the decline in permeate flux was due to membrane fouling, or the pores being wetted. Banat and Simandl [33] analysed the effect of long operation (two months) on the permeate flux for tap water (297 μS/cm). They found that the flux increased during the first 50 h, and then fell for 160 h before reaching a steady state. The permeate conductivity was steady at about 3 μS/cm. For seawater, the experiment was conducted for 10 days. The flux declined until it reached a steady state [5]. Drioli and Yonglie [125] reached to the same result, when 1 mol NaCl had been used for 6 days.

11. Conclusions

Membrane Distillation (MD) is a promising technology for separation and purification processes. It is a thermally-driven separation process, in which only vapour molecules are able to pass through a porous hydrophobic membrane. Unlike normal membrane processes which operate on temperature difference, MD separation is driven by the vapour pressure difference existing between the porous hydrophobic membrane surfaces.

In this review, membrane configuration, membrane characteristics, membrane modules, mass and heat transport mechanisms, thermal efficiency, fouling and operating parameters were covered. This review reveals that some potential research areas pertinent to MD deserve further exploration. In particular:

- Most of conducted MD studies are based on lab scale experimentation to investigate the influence of operating conditions. Large-scale MD studies covering industrial applications are still scarce and, therefore, represents an interesting area of research.
- With the exception of DCMD, which has been widely studied, other MD configurations have not been equally explored, hence more focus on other MD configuration is required.
- There are limited studies of the influence of high concentration solution on the mass and heat transfer mechanisms. Consequently, the effect of high concentration should be examined more.
- On the technology front and in view of the vital membrane hydrophobicity feature, development of microporous membranes with high hydrophobic character deserves more emphasis.
- The energy consumption of MD and the effect of operating parameters require further investigation as the available research data on this research area look limited based on the review presented here.

Acknowledgement

Authors would like to thank King Abdul Aziz City for Science and Technology (KACST) for funding Mr Abdullah Alkhudhiri.

References

[1] M. Gryta, K. Karakulski, A.W. Morawski, Purification of oily wastewater by hybrid UF/MD, Water Res. 35 (15) (2001) 3665–3669.
[2] A. Criscuoli, E. Drioli, Energetic and exergetic analysis of an integrated membrane desalination system, Desalination 124 (1–3) (1999) 243–249.
[3] H. Kurokawa, T. Sawa, Heat recovery characteristics of membrane distillation, Heat transfer-Japanese Research 25 (1996) 135–150.
[4] J. Blanco Gálvez, L. García-Rodríguez, I. Martín-Mateos, Seawater desalination by an innovative solar-powered membrane distillation system: the MEDESOL project, Desalination 246 (1–3) (2009) 567–576.
[5] F.A. Banat, J. Simandl, Desalination by membrane distillation: a parametric study, Sep. Sci. Technol. 33 (2) (1998) 201–226.
[6] M.C. García-Payo, M.A. Izquierdo-Gil, C. Fernández-Pineda, Air gap membrane distillation of aqueous alcohol solutions, J. Membr. Sci. 169 (1) (2000) 61–80.
[7] P.P. Zolotarev, et al., Treatment of waste water for removing heavy metals by membrane distillation, J. Hazard. Mater. 37 (1) (1994) 77–82.
[8] G. Zakrzewska-Trznadel, M. Harasimowicz, A.G. Chmielewski, Concentration of radioactive components in liquid low-level radioactive waste by membrane distillation, J. Membr. Sci. 163 (2) (1999) 257–264.
[9] E. Curcio, E. Drioli, Membrane distillation and related operations — a review, Sep. Purif. Rev. 34 (1) (2005) 35–86.
[10] K.W. Lawson, D.R. Lloyd, Membrane distillation, J. Membr. Sci. 124 (1) (1997) 1–25.
[11] V.D. Alves, I.M. Coelhoso, Orange juice concentration by osmotic evaporation and membrane distillation: a comparative study, J. Food Eng. 74 (1) (2006) 125–133.
[12] S. Gunko, et al., Concentration of apple juice using direct contact membrane distillation, Desalination 190 (1–3) (2006) 117–124.
[13] M.P. Godino, et al., Water production from brines by membrane distillation, Desalination 108 (1–3) (1997) 91–97.
[14] S.T. Hsu, K.T. Cheng, J.S. Chiou, Seawater desalination by direct contact membrane distillation, Desalination 143 (3) (2002) 279–287.
[15] V. Calabro, B.L. Jiao, E. Drioli, Theoretical and experimental study on membrane distillation in the concentration of orange juice, Ind. Eng. Chem. Res. 33 (7) (1994) 1803–1808.
[16] M. Tomaszewska, M. Gryta, A.W. Morawski, Study on the concentration of acids by membrane distillation, J. Membr. Sci. 102 (1995) 113–122.
[17] J. Walton, et al., Solar and waste heat desalination by membrane distillation, College of Engineering University of Texas, El Paso, 2004.
[18] S. Kimura, S.-I. Nakao, S.-I. Shimatani, Transport phenomena in membrane distillation, J. Membr. Sci. 33 (3) (1987) 285–298.
[19] F.A. Banat, J. Simandl, Membrane distillation for dilute ethanol: separation from aqueous streams, J. Membr. Sci. 163 (2) (1999) 333–348.

[20] M. Khayet, Membranes and theoretical modeling of membrane distillation: A review, Adv. Colloid Interface Sci. 164 (1–2) (2011) 56–88.
[21] M.C. García-Payo, et al., Separation of binary mixtures by thermostatic sweeping gas membrane distillation: II. Experimental results with aqueous formic acid solutions, J. Membr. Sci. 198 (2) (2002) 197–210.
[22] S. Bandini, G.C. Sarti, Heat and mass transport resistances in vacuum membrane distillation per drop, AIChE Journal 45 (1999) 1422–1433.
[23] S. Bandini, C. Gostoli, G.C. Sarti, Separation efficiency in vacuum membrane distillation, J. Membr. Sci. 73 (2–3) (1992) 217–229.
[24] K.W. Lawson, D.R. Lloyd, Membrane distillation. I. Module design and performance evaluation using vacuum membrane distillation, J. Membr. Sci. 120 (1) (1996) 111–121.
[25] C. Gostoli, G.C. Sarti, Separation of liquid mixtures by membrane distillation, J. Membr. Sci. 41 (1989) 211–224.
[26] M.C. García-Payo, M.A. Izquierdo-Gil, C. Fernández-Pineda, Wetting study of hydrophobic membranes via liquid entry pressure measurements with aqueous alcohol solutions, J. Colloid Interface Sci. 230 (2) (2000) 420–431.
[27] A.C.M. Franken, et al., Wetting criteria for the applicability of membrane distillation, J. Membr. Sci. 33 (3) (1987) 315–328.
[28] M. Tomaszewska, Preparation and properties of flat-sheet membranes from poly(vinylidene fluoride) for membrane distillation, Desalination 104 (1–2) (1996) 1–11.
[29] S. Khemakhem, R.B. Amar, Grafting of Fluoroalkylsilanes on Microfiltration Tunisian Clay Membrane, Ceram. Int. (2011) doi:10.1016/j.ceramin., 2011.04.128.
[30] S. Cerneaux, et al., Comparison of various membrane distillation methods for desalination using hydrophobic ceramic membranes, J. Membr. Sci. 337 (1–2) (2009) 55–60.
[31] J. Zhang, et al., Identification of material and physical features of membrane distillation membranes for high performance desalination, J. Membr. Sci. 349 (1–2) (2010) 295–303.
[32] A.M. Alklaibi, N. Lior, Membrane-distillation desalination: status and potential, Desalination 171 (2) (2005) 111–131.
[33] F.A. Banat, J. Simandl, Theoretical and experimental study in membrane distillation, Desalination 95 (1) (1994) 39–52.
[34] K. Schneider, et al., Membranes and modules for transmembrane distillation, J. Membr. Sci. 39 (1) (1988) 25–42.
[35] M. Khayet, K.C. Khulbe, T. Matsuura, Characterization of membranes for membrane distillation by atomic force microscopy and estimation of their water vapor transfer coefficients in vacuum membrane distillation process, J. Membr. Sci. 238 (1–2) (2004) 199–211.
[36] M. Khayet, N.N. Li, A.G. Fane, W.S. winston Ho, Membrane Distillation, Advance Membrane Technology and Applications, John Wiley, New Jersey, 2008.
[37] M. Mulder, Basic Principles of membrane Technology, seconde ed. Kluwer Academic Publishers, Netherlands, 2003.
[38] F. Laganà, G. Barbieri, E. Drioli, Direct contact membrane distillation: modelling and concentration experiments, J. Membr. Sci. 166 (1) (2000) 1–11.
[39] M. Khayet, T. Matsuura, Preparation and characterization of polyvinylidene fluoride membranes for membrane distillation, Ind. Eng. Chem. Res. 40 (24) (2001) 5710–5718.
[40] M.S. El-Bourawi, et al., A framework for better understanding membrane distillation separation process, J. Membr. Sci. 285 (1–2) (2006) 4–29.
[41] S. Srisurichan, R. Jiraratananon, A.G. Fane, Mass transfer mechanisms and transport resistances in direct contact membrane distillation process, J. Membr. Sci. 277 (1–2) (2006) 186–194.
[42] A.O. Imdakm, T. Matsuura, Simulation of heat and mass transfer in direct contact membrane distillation (MD): the effect of membrane physical properties, J. Membr. Sci. 262 (1–2) (2005) 117–128.
[43] M. Khayet, A. Velázquez, J.I. Mengual, Modelling mass transport through a porous partition: effect of pore size distribution, J. Non-Equilib. Thermodyn 29 (3) (2004) 279–299.
[44] J. Phattaranawik, R. Jiraratananon, A.G. Fane, Effect of pore size distribution and air flux on mass transport in direct contact membrane distillation, J. Membr. Sci. 215 (1–2) (2003) 75–85.
[45] L. Martínez, et al., Estimation of vapor transfer coefficient of hydrophobic porous membranes for applications in membrane distillation, Sep. Purif. Technol. 33 (1) (2003) 45–55.
[46] A.O. Imdakm, T. Matsuura, A Monte Carlo simulation model for membrane distillation processes: direct contact (MD), J. Membr. Sci. 237 (1–2) (2004) 51–59.
[47] M. Khayet, J.I. Mengual, G. Zakrzewska-Trznadel, Direct contact membrane distillation for nuclear desalination. Part I: Review of membranes used in membrane distillation and methods for their characterisation Int, Nucl. Des. 1 (4) (2005) 435–449.
[48] M. Khayet, T. Matsuura, Pervaporation and vacuum membrane distillation processes: Modeling and experiments, Ind. Eng. Chem. Res. 50 (2004) 1697–1712.
[49] J. Kong, K. Li, An improved gas permeation method for characterising and predicting the performance of microporous asymmetric hollow fibre membranes used in gas absorption, J. Membr. Sci. 182 (1–2) (2001) 271–281.
[50] J. Phattaranawik, R. Jiraratananon, A.G. Fane, Heat transport and membrane distillation coefficients in direct contact membrane distillation, J. Membr. Sci. 212 (1–2) (2003) 177–193.
[51] C.A. Sperati, E.I. DuPont de Nemours, Polymer Handbook, in: J. Brandrup, E.H. Immergut (Eds.), second ed., John Wiley, USA, 1975.
[52] A.S. Jönsson, R. Wimmerstedt, A.C. Harrysson, Membrane distillation — a theoretical study of evaporation through microporous membranes, Desalination 56 (1985) 237–249.
[53] M. Khayet, et al., Design of novel direct contact membrane distillation membranes, Desalination 192 (1–3) (2006) 105–111.
[54] C. Feng, et al., Preparation and properties of microporous membrane from poly(-vinylidene fluoride-co-tetrafluoroethylene) (F2.4) for membrane distillation, J. Membr. Sci. 237 (1–2) (2004) 15–24.
[55] Y. Wu, et al., Surface-modified hydrophilic membranes in membrane distillation, J. Membr. Sci. 72 (2) (1992) 189–196.
[56] N. Hengl, et al., Study of a new membrane evaporator with a hydrophobic metallic membrane, J. Membr. Sci. 289 (1–2) (2007) 169–177.
[57] K.W. Lawson, M.S. Hall, D.R. Lloyd, Compaction of microporous membranes used in membrane distillation. I. Effect on gas permeability, J. Membr. Sci. 101 (1–2) (1995) 99–108.
[58] A. Kullab, A. Martin, Membrane distillation and applications for water purification in thermal cogeneration plants, Sep. Purif. Technol. 76 (3) (2011) 231–237.
[59] M. Khayet, A. Velázquez, J.I. Mengual, Direct contact membrane distillation of humic acid solutions, J. Membr. Sci. 240 (1–2) (2004) 123–128.
[60] S. Srisurichan, R. Jiraratananon, A.G. Fane, Humic acid fouling in the membrane distillation process, Desalination 174 (1) (2005) 63–72.
[61] P. Termpiyakul, R. Jiraratananon, S. Srisurichan, Heat and mass transfer characteristics of a direct contact membrane distillation process for desalination, Desalination 177 (1–3) (2005) 133–141.
[62] Z. Ding, R. Ma, A.G. Fane, A new model for mass transfer in direct contact membrane distillation, Desalination 151 (3) (2003) 217–227.
[63] R.W. Schofield, et al., Factors affecting flux in membrane distillation, Desalination 77 (1990) 279–294.
[64] A. El-Abbassi, et al., Concentration of olive mill wastewater by membrane distillation for polyphenols recovery, Desalination 245 (1–3) (2009) 670–674.
[65] Y. Yun, et al., Direct contact membrane distillation mechanism for high concentration NaCl solutions, Desalination 188 (1–3) (2006) 251–262.
[66] K. Sakai, et al., Effects of temperature and concentration polarization on water vapour permeability for blood in membrane distillation, Chem. Eng. J. 38 (3) (1988) B33–B39.
[67] H. Kurokawa, et al., Vapor permeate characteristics of membrane distillation, Sep. Sci. Technol. 25 (13) (1990) 1349–1359.
[68] M. Khayet, P. Godino, J.I. Mengual, Nature of flow on sweeping gas membrane distillation, J. Membr. Sci. 170 (2) (2000) 243–255.
[69] M. Khayet, P. Godino, J.I. Mengual, Theory and experiments on sweeping gas membrane distillation, J. Membr. Sci. 165 (2) (2000) 261–272.
[70] Y. Fujii, et al., Selectivity and characteristics of direct contact membrane distillation type experiment. I. Permeability and selectivity through dried hydrophobic fine porous membranes, J. Membr. Sci. 72 (1) (1992) 53–72.
[71] M. Gryta, Concentration of saline wastewater from the production of heparin, Desalination 129 (1) (2000) 35–44.
[72] M.D. Kennedy, et al., Water treatment by microfiltration and ultrafiltration, in: A. Li, et al., (Eds.), Advance Membrane Technology and Application, John Wiley, New Jersey, 2008.
[73] E. drioli,, V. Calabro, Y. Wu, Microporous membranes in membrane distillation, Pure Appl. Chem. 58 (12) (1986) 1657–1662.
[74] E. Drioli, Y. Wu, V. Calabro, Membrane distillation in the treatment of aqueous solutions, J. Membr. Sci. 33 (3) (1987) 277–284.
[75] R.W. Schofield, A.G. Fane, C.J.D. Fell, Heat and mass transfer in membrane distillation, J. Membr. Sci. 33 (3) (1987) 299–313.
[76] L. Martínez, J.M. Rodríguez-Maroto, On transport resistances in direct contact membrane distillation, J. Membr. Sci. 295 (1–2) (2007) 28–39.
[77] P. Godino, L. Peña, J.I. Mengual, Membrane distillation: theory and experiments, J. Membr. Sci. 121 (1) (1996) 83–93.
[78] S. Al-Obaidani, et al., Potential of membrane distillation in seawater desalination: thermal efficiency, sensitivity study and cost estimation, J. Membr. Sci. 323 (1) (2008) 85–98.
[79] R.W. Schofield, A.G. Fane, C.J.D. Fell, Gas and vapour transport through microporous membranes. II. Membrane distillation, J. Membr. Sci. 53 (1–2) (1990) 173–185.
[80] E. Cussler, Diffusion mass transfer in fluid systems, Second ed. Cambridge University Press, 1997.
[81] C. Geankoplis, Transport Process and Separation Principles, Fourth ed. Prentice Hall, New Jersey, 2003.
[82] C.M. Guijt, et al., Modelling of a transmembrane evaporation module for desalination of seawater, Desalination 126 (1–3) (1999) 119–125.
[83] R.W. Schofield, A.G. Fane, C.J.D. Fell, Gas and vapour transport through microporous membranes. I. Knudsen–Poiseuille transition, J. Membr. Sci. 53 (1–2) (1990) 159–171.
[84] A.G. Fane, R.W. Schofield, C.J.D. Fell, The efficient use of energy in membrane distillation, Desalination 64 (1987) 231–243.
[85] L. Martínez, Comparison of membrane distillation performance using different feeds, Desalination 168 (2004) 359–365.
[86] V. Gekas, B. Hallström, Mass transfer in the membrane concentration polarization layer under turbulent cross flow: I. Critical literature review and adaptation of existing Sherwood correlations to membrane operations, J. Membr. Sci. 30 (2) (1987) 153–170.
[87] C.M. Tun, et al., Membrane distillation crystallization of concentrated salts-flux and crystal formation, J. Membr. Sci. 257 (1–2) (2005) 144–155.
[88] G.L. Liu, et al., Theoretical and experimental studies on air gap membrane distillation, Heat and Mass Transfer 34 (4) (1998) 329–335.
[89] A.M. Alklaibi, N. Lior, Transport analysis of air-gap membrane distillation, J. Membr. Sci. 255 (1–2) (2005) 239–253.
[90] M.N. Chernyshov, G.W. Meindersma, A.B. de Haan, Modelling temperature and salt concentration distribution in membrane distillation feed channel, Desalination 157 (1–3) (2003) 315–324.

[91] R. Brid, w. Stewart, E. Lightfoot, Transport Phenomena, Second ed. John Wiley, 2001.
[92] S. Bouguecha, R. Chouikh, M. Dhahbi, Numerical study of the coupled heat and mass transfer in membrane distillation, Desalination 152 (1–3) (2003) 245–252.
[93] F.A. Banat, et al., Application of Stefan-Maxwell approach to azeotropic separation by membrane distillation, Chem. Eng. J. 73 (1) (1999) 71–75.
[94] F.A. Banat, et al., Theoretical investigation of membrane distillation role in breaking the formic acid-water azeotropic point: comparison between Fickian and Stefan-Maxwell-based models, Int. Commun. Heat Mass Transf. 26 (6) (1999) 879–888.
[95] S. Bandini, A. Saavedra, G.C. Sarti, Vacuum membrane distillation: Experiments and modeling, AIChE Journal 43 (1997) 398–408.
[96] J.I. Mengual, M. Khayet, M.P. Godino, Heat and mass transfer in vacuum membrane distillation, Int. J. Heat Mass Transf. 47 (4) (2004) 865–875.
[97] L. Martinez-Diez, M.I.V. Gonzalez, Effects of polarization on mass transport through hydrophobic porous membranes, Ind. Eng. Chem. Res. 37 (10) (1998) 4128–4135.
[98] M. Sudoh, et al., Effects of thermal and concentration boundary layers on vapor permeation in membrane distillation of aqueous lithium bromide solution, J. Membr. Sci. 131 (1–2) (1997) 1–7.
[99] L. Martínez-Díez, M.I. Vázquez-Gonzàlez, Temperature polarization in mass transport through hydrophobic porous, membranes, AIChE Journal 42 (1996) 1844–1852.
[100] L. Martínez, J.M. Rodríguez-Maroto, Effects of membrane and module design improvements on flux in direct contact membrane distillation, Desalination 205 (1–3) (2007) 97–103.
[101] L. Martínez-Díez, M.I. Vázquez-González, Temperature and concentration polarization in membrane distillation of aqueous salt solutions, J. Membr. Sci. 156 (2) (1999) 265–273.
[102] J. Phattaranawik, R. Jiraratananon, Direct contact membrane distillation: effect of mass transfer on heat transfer, J. Membr. Sci. 188 (1) (2001) 137–143.
[103] M. Qtaishat, et al., Heat and mass transfer analysis in direct contact membrane distillation, Desalination 219 (1–3) (2008) 272–292.
[104] M. Gryta, M. Tomaszewska, Heat transport in the membrane distillation process, J. Membr. Sci. 144 (1–2) (1998) 211–222.
[105] V. Calabrò, E. Drioli, F. Matera, Membrane distillation in the textile wastewater treatment, Desalination 83 (1–3) (1991) 209–224.
[106] M. Gryta, M. Tomaszewska, A.W. Morawski, Membrane distillation with laminar flow, Sep. Purif. Technol. 11 (2) (1997) 93–101.
[107] T.-C. Chen, C.-D. Ho, H.-M. Yeh, Theoretical modeling and experimental analysis of direct contact membrane distillation, J. Membr. Sci. 330 (1–2) (2009) 279–287.
[108] M.A. Izquierdo-Gil, M.C. García-Payo, C. Fernández-Pineda, Air gap membrane distillation of sucrose aqueous solutions, J. Membr. Sci. 155 (2) (1999) 291–307.
[109] M. Tomaszewska, M. Gryta, A.W. Morawski, A study of separation by the direct-contact membrane distillation process, Sep. Technol. 4 (4) (1994) 244–248.
[110] M.A. Izquierdo-Gil, C. Fernández-Pineda, M.G. Lorenz, Flow rate influence on direct contact membrane distillation experiments: different empirical correlations for Nusselt number, J. Membr. Sci. 321 (2) (2008) 356–363.
[111] G.C. Sarti, C. Gostoli, S. Matulli, Low energy cost desalination processes using hydrophobic membranes, Desalination 56 (1985) 277–286.
[112] S. Bandini, C. Gostoli, G.C. Sarti, Role of heat and mass transfer in membrane distillation process, Desalination 81 (1–3) (1991) 91–106.
[113] L. Martínez-Díez, F.J. Florido-Díaz, M.I. Vázquez-González, Study of evaporation efficiency in membrane distillation, Desalination 126 (1–3) (1999) 193–198.
[114] A. Criscuoli, M.C. Carnevale, E. Drioli, Evaluation of energy requirements in membrane distillation, Chem. Eng. Process. Process Intensif. 47 (7) (2008) 1098–1105.
[115] Z. Ding, et al., Analysis of a solar-powered membrane distillation system, Desalination 172 (1) (2005) 27–40.
[116] P.A. Hogan, et al., Desalination by solar heated membrane distillation, Desalination 81 (1–3) (1991) 81–90.
[117] S. Shirazi, C.-J. Lin, D. Chen, Inorganic fouling of pressure-driven membrane processes -A critical review, Desalination 250 (1) (2010) 236–248.
[118] M. Gryta, Long-term performance of membrane distillation process, J. Membr. Sci. 265 (1–2) (2005) 153–159.
[119] M. Gryta, Fouling in direct contact membrane distillation process, J. Membr. Sci. 325 (1) (2008) 383–394.
[120] M. Matheswaran, et al., Factors affecting flux and water separation performance in air gap membrane distillation, J. Ind. Eng. Chem. 13 (6) (2007) 965–970.
[121] M. Safavi, T. Mohammadi, High-salinity water desalination using VMD, Chem. Eng. J. 149 (1–3) (2009) 191–195.
[122] S. Kubota, et al., Experiments on seawater desalination by membrane distillation, Desalination 69 (1) (1988) 19–26.
[123] H. Udriot, A. Araque, U. von Stockar, Azeotropic mixtures may be broken by membrane distillation, Chem. Eng. J. Biochem. Eng. J. 54 (2) (1994) 87–93.
[124] Z. Xiuli, et al., Mathematical model of gas permeation through PTFE porous membrane and the effect of membrane, Chinese J. Chem. Eng. 11 (4) (2003) 383–387.
[125] E. Drioli, Y. Wu, Membrane distillation: an experimental study, Desalination 53 (1–3) (1985) 339–346.